Cell-cycle dependent inhibition of BRCA1 signaling by the lysine methyltransferase SET8

Yannick PEREZ[1,2], Fatima ALHOURANI[1,2], Julie PATOUILLARD[1], Cyril RIBEYRE[2,3,4], Marion LARROQUE[1], Véronique BALDIN[1,2,4], David LLERES[2,4,5], Charlotte GRIMAUD[1,2,4*] and Eric JULIEN[1,2,4*]

1. Institut de Recherche en Cancérologie de Montpellier (IRCM), INSERM U1194, Institut Régional du Cancer (ICM), Montpellier F-34298, France

2. University of Montpellier, Montpellier, F-34090, France

3. Institut de Génétique Humaine (IGH), CNRS UMR 9002, Montpellier F-34996, France

4. Centre National de la Recherche Scientifique (CNRS), F-34293, Montpellier, France

5. Institut de Génétique Moléculaire de Montpellier (IGMM), CNRS UMR 5535, Montpellier F34293, France.

* co-last authors

Author correspondence : eric.julien@inserm.fr

SUMMARY

Although the inverse affinities of 53BP1 and BRCA1-BARD1 complexes for distinct methylation sates of lysine (K) 20 at histone H4 have underscored a role of this epigenetic mark in the regulation of DNA-repair pathways choice, how the different H4K20 methyltransferases are involved remained unclear. Here, we show that the replication-coupled degradation of the lysine methyltransferase SET8 responsible for H4K20 mono-methylation (H4K20me1) is primordial for the onset of the recombinogenic functions of BRCA1 during unperturbed DNA replication. Indeed, independently of other H4K20me states, we determined that the SET8-induced switch from un-methyl to mono-methyl H4K20 followed by the activation of the ubiquitin ligase RNF168 constitutes a turn-off signal of homologous recombination by tipping the balance from BRCA1-BARD1 to 53BP1 complexes on post-replicated chromatin. Conversely, the lack of SET8 and the absence of H4K20 monomethylation after DNA replication led to an inaccurate chromatin accumulation of BRCA1 at the exit of mitosis, which contributes to the improper progression from G1 to S-phase in daughter cells. Altogether, these results establish the activity of SET8 on chromatin as the primary inhibitory lock of BRCA1-mediated HR pathway during the cell cycle.

INTRODUCTION

The genome of eukaryotic cells is constantly challenged by variety of DNA insults, which can occur in response to exogenous agents or accidentally during DNA-dependent processes (Scully et al. 2019). Double-strand breaks (DSBs) represent the most detrimental lesions, because failure to eliminate them can lead to cell death or a wide variety of genetic alterations (Xu and Xu 2020). To deal with this threat, cells have evolved an elaborate DNA repair network where homologous recombination (HR) and non-homologous end joining (NHEJ) are the two major pathways used for repairing DSBs (Hustedt and Durocher 2017; Scully et al. 2019). In contrast to NHEJ, HR usually depends on the presence of a sister chromatid produced by DNA replication, as it provides an undamaged homologous template for repair of both broken strands. The use of HR is therefore closely linked to S and G2 phases of the cell cycle (Hustedt et Durocher 2017). Furthermore, most of HR factors are naturally found enriched in the vicinity of replication forks, suggesting that they play important role in the stability of genome during S-phase and making HR as the favored repair pathway to deal with replication-associated DNA lesions (Kolinjivadi et al. 2017). However, while the cascade of events that lead to the activation of homologous recombination is extensively studied in the context of exogenous DNA lesions, less is known about the mechanisms that regulate HR during unperturbed S-phase progression. Notably, how HR signaling pathway is specifically restrained to both S and G2 phases of the cell cycle is still poorly understood. Yet, these mechanisms are likely essential, since inaccurate activation or misuse in HR pathways during the other phases of the cell cycle can cause deleterious outcomes associated with cancer (Toh et Ngeow 2021; Jeggo et Löbrich 2015).

A critical determinant for the regulation of HR signaling pathway is the balanced activities between the pro-NHEJ protein 53BP1 and the HR-promoting heterodimer formed by BRCA1 and BARD1 during the cell cycle (Hustedt and Durocher 2017; Scully et al. 2019). Upon DNA damage, 53BP1 accumulates at DSB sites by recognizing notably nucleosomes marked by the di-methylation of histone H4 at lysine 20 (H4K20me2) and to lesser extent ubiquitylation of histone H2A at lysine 15 (Fradet-Turcotte et al. 2013). This 53BP1 accumulation on damaged chromatin limits HR by antagonizing the DNA end resection activity of BRCA1-BARD1 and thus the subsequent loading of RAD51 that catalyzes the repair reaction by recombination (Tarsounas and Sung 2020). As cells progress through S phase, the ability of 53BP1 to accumulate around DNA breaks decline. This has been notably attributed to the replication-coupled dilution of H4K20me2 mark on post-replicated chromatin (Michelena et al. 2021; Tarsounas et Sung 2020). Yet, 53BP1 can also interact with histone H4K20 mono-methylation (H4K20me1) and tri-methylation (H4K20me3) (Botuyan et al. 2006; Svobodová et al. 2018), thereby questioning this model. Conversely, the lack of methylation of H4K20 (H4K20me0) is a mark of post-replicative chromatin specifically recognized by the ankyrin domain of BARD1, which contributes to BRCA1 recruitment and the eviction of 53BP1 when sister chromatid is available for HR repair (Nakamura et al. 2019; Witus et al. 2022). Thus, the inverse affinities of 53BP1 and BARD1 for distinct methylation sates of histone H4K20 have underscored a potential key role of this lysine methylation in the regulation of DNA repair pathways choice during the cell cycle. However, this hypothesis has been explored so far only in response to exogenous DNA damaging agents and never been validated in a more physiological and unchallenged context. Furthermore, the H4K20 enzymes

responsible and the biological significance of different H4K20me states in the cell-cycle regulatory interplay between 53BP1 and BRCA1 still remain poorly understood.

In this work, we provide evidences that the histone H4K20 mono-methyltransferase SET8 on its own works as the primary turn-off timer of BRCA1 recombinogenic functions. SET8 activity appears essential to avoid improper BRCA1 HR activity on chromatin outside of S and G2 phases. This inhibitory role on BRCA1 functions is linked to the single conversion of H4K20me0 to H4K20me1 followed by the chromatin binding of the ubiquitin ligase RNF168, which together contributes to the switch from BRCA1 to the anti-recombinogenic functions of 53BP1 on post-replicated chromatin.

RESULTS

PCNA-mediated SET8 degradation is required for H4K20me0 enrichment on post-replicated chromatin. Previous studies showed that the newly incorporated histones H4 during S-phase remained unmethylated at lysine 20 (H4K20me0) until the onset of mitosis (Alabert et al. 2015). The absence of methylation of newly synthetized histone H4 may be related to the higher activity of H4K20 demethylases at the onset of DNA replication, as suggested by previous studies on PHF8 and hHR23 enzymes (Cao et al. 2020; Liu et al. 2010). An alternative but not mutually exclusive possibility is that the H4K20me0 enrichment during S-phase could be also favored by the replication-coupled degradation of the lysine methyltransferase SET8 responsible for H4K20 mono-methylation (H4K20me1), a prerequisite for higher H4K20me states (H4K20me2/me3) induced by SUV4-20H enzymes (Beck et al. 2012, 4; Brustel et al. 2011; Jørgensen et al. 2013). To explore further this second possibility, we used an U2OS cell line harboring a tetracycline(Tet)-inducible FLAG-SET8^{PIPmut} enzyme

unable to interact with PCNA and thus resistant to the protein destruction mediated by the CRL4^{CTD2} complex during S-phase (Centore et al. 2010; Oda et al. 2010; Tardat et al. 2010). The advantage of this Tet-inducible SET8 cellular model is that we can efficiently synchronized cells and study the immediate impact of FLAG-SET8^{PIPmut} expression on chromatin without inducing the re-replication phenotype associated with long-term SET8 stabilization as previously described (Beck et al. 2012; Tardat et al. 2010). Thus, U2OS cells were first synchronized at G1/S transition by thymidine block and then the expression of FLAG-SET8^{PIPmut} was induced by tetracycline treatment for at least 2 hours before release into S-phase. Although displaying a slight delay in S-phase entry, tetracycline-treated cells then progressed similarly in S-phase compared to untreated cells as observed by FACS analysis (Figure 1A). As cells progressed into S-phase, immunoblot analysis showed that the levels of endogenous SET8, but not of FLAG-SET8^{PIPmut} mutant, declined rapidly as expected (Figure 1B). Consistent with previous studies (Rice et al. 2002; Tardat et al. 2010; Alabert et al. 2015), the lack of SET8 in control cells was accompanied by the decrease in the steady state levels of H4K20me1 and the concomitant accumulation of unmethylated H4K20 mark (H4K20me0) (Figure 1B, left panels). In contrast, the expression of the non-degradable FLAG-SET8^{PIPmut} mutant was sufficient to prevent the decline of H4K20me1 and the appearance of H4K20me0 in tetracycline-treated cells (Figure 1B, right panels). Since H4K20me0 is a hallmark of post-replicated chromatin, we hypothesized that FLAG-SET8^{PIPmut} expression on its own was sufficient to trigger *de novo* H4K20me1 on newly incorporated histones H4 in the wake of replication forks. To verify this hypothesis, asynchronous control and tetracycline-treated U2OS cells were pulse-labelled with EdU for 20 minutes and treated with formaldehyde to cross-link protein-DNA complexes. After covalent linkage of biotin-azide to EdU using click

chemistry, EdU-labelled DNA and associated proteins were isolated by iPOND (Isolation of Proteins on Nascent DNA) method and then analyzed by immunoblotting (Dungrawala et Cortez 2015). The procedure without click-it reaction served as negative controls. As shown in Figure 1C, immunoblot analysis showed similar levels of histones and PCNA in untreated and tetracycline-treated U2OS samples after click-it reaction, thereby indicating that replisome and chromatin proteins associated with EdU-labelled DNA were efficiently and similarly captured in control and FLAG-SET8^{PIPmut} expressing cells. In these conditions, analysis of H4K20me states by immunoblot revealed a loss of H4K20me0 with a concomitant gain of H4K20me1 in nascent chromatin upon SET8^{PIPmut} expression, while the levels of H4K20me2 and H4K20me3, which mainly corresponded to recycled histones H4 (Alabert et al. 2015), remained largely unchanged (Figure 1C). Altogether, these results demonstrate that the expression of a non-degradable SET8 enzyme is sufficient to prevent H4K20me0 accumulation by inducing its premature conversion to H4K20me1 on newly incorporated histones H4. Hence, the natural enrichment of H4K20me0 on post-replicated chromatin largely depends on the replication-coupled degradation of SET8 in U2OS cells.

The premature switch from H4K20me0 to H4K20me1 modify nascent chromatin composition. To determine whether the switch from H4K20me0 to H4K20me1 impacts on the protein composition of nascent chromatin formed in the wake of replication forks, proteins isolated by iPOND approach were analyzed by mass spectrometry (MS). iPOND purification without click-it reaction served as controls to identify non-specific protein binding to EdU labelled DNA in untreated and tetracycline-treated conditions. Hence, in this IPOND-MS experiment, we identified 547 proteins

specifically enriched on Edu-labelled DNA in control untreated cells (-TET), while 595 proteins were identified in replicating cells treated with tetracyline (+TET) and that expressed the non-degradable FLAG-SET8^{PIPmut} protein (Figure 1D). Of the total proteins identified, 840 of them (73.5%) were common in both cellular conditions (Figure 1D). They mostly corresponded to proteins already known to be enriched at replication forks and functionally linked to DNA replication, DNA repair, chromatin structure and RNA regulation (Wessel et al. 2019; Ribeyre et al. 2016). Interestingly, however, 197 proteins were found specifically associated with EdU-labelled DNA in response to FLAG-SET8^{PIPmut} expression, including SET8 itself, while 105 proteins normally enriched on newly synthetized DNA in control cells were lost upon SET8 stabilization (Figures 1E-1H). Gene ontology analysis revealed an over-representation of proteins involved in mRNA metabolism, chromatin organization and DNA repair pathways in both cellular conditions (Figures 1E and 1G). Looking closer at the list of proteins involved in DNA repair and chromatin-related pathways, we noticed the gain of 53PB1, HDAC2, BABAM2, SMC5 and several non-SMC family proteins upon FLAG-SET8^{PIPmut} expression (Figure 1E). In contrast, we observed the loss of BRCA1 and several other DNA repair-associated proteins such as PARP2, ERCC2, OTUB1 or TONSL. This last result was consistent with previous studies showing the ability of TONSL to interact *in vitro* with peptides and nucleosomes harboring H4K20me0 marks but not H4K20me1 (Nakamura et al. 2019; Saredi et al. 2016). Altogether, these results suggest that the premature stabilization of SET8 and the subsequent mono-methylation of lysine 20 on newly incorporated histones H4 were sufficient to modify significantly the composition of post-replicated chromatin, notably by altering the binding of several key proteins in chromatin and DNA repair regulatory pathways.

SET8 upregulation impairs the focal accumulation of HR proteins during S-phase. During S-phase and even in absence of exogenous DNA damage, BRCA1 spontaneously form nuclear foci to support replication machinery and to ensure genome stability (Aze et al. 2013; Kolinjivadi et al. 2017). To determine whether unscheduled SET8 activity impairs BRCA1 foci formation and instead could favor 53BP1 focal accumulation as suggested by our iPOND-MS data (Figure 1), we examined by immunofluorescence the number of BRCA1 and 53BP1 foci in control and FLAG-SET8^{PIPmut} replicating cells. We also examined by immunofluorescence the levels of BARD1 and RAD51 focal accumulation, since BARD1 forms a heterodimer with BRCA1 and its binding to H4K20me0 contributes to the subsequent recruitment of RAD51 on replicated DNA (Nakamura et al. 2019). After treatment or not with tetracycline to induce FLAG-SET8^{PIPmut} expression, cells were pulse-labelled with EdU for 30 minutes before fixation. Fixed cells were then treated with click-it chemistry to reveal EdU incorporation in replicating cells and then co-stained with BARD1, BRCA1, Rad51 or 53BP1 antibodies. The representative images of the results are shown in Figure 2A and their quantifications are shown in Figures 2B and in Supplementary Figure S1A. Consistent with FACS analysis (Figure 1A), the EdU staining was similar between the control and FLAG-SET8^{PIPmut} replicating cells. As expected, RAD51, BARD1 and BRCA1 nuclear foci were detected in control replicating cells (Figure 2A and Figure S1A). We also noticed that these control cells displayed few and disperse 53BP1 foci (Figure 2A). In contrast, BRCA1, BARD1 and RAD51 nuclear foci were almost abolished in replicating cells upon FLAG-SET8^{PIPmut} expression, whereas the number and size of 53BP1 nuclear foci were strongly increased (Figures 2A and 2B, Figure S1B).

To demonstrate that the loss of nuclear HR foci is related to the methyltransferase activity of SET8^{PIPmut} protein, U2OS cells were transduced with pBabe retroviral vectors encoding the active FLAG-SET8^{PIPmut} or its catalytic dead version FLAG-SET8$^{PIPmut+SETmut}$. Three days after retroviral infection, the levels of RAD51 and 53BP1 nuclear foci in replicating cells were examined by immunofluorescence. As shown in figures 2C and 2D, the expression of the inactive FLAG-SET8$^{PIPmut+SETmut}$, but not of FLAG-SET8^{PIPmut}, failed to reduce RAD51 foci formation and to stimulate 53BP1 focal accumulation during S-phase. Noted of, defects in RAD51 foci formation during DNA replication are sufficient to impair homologous recombination (HR) and trigger genome instability (Bhowmick et al. 2022, 51; Costanzo et al. 2011 ; Feu et al. 2022). Consistent with this, we noticed later the appearance of γH2A.X foci that mostly coincided with the presence of 53BP1 foci in FLAG-SET8^{PIPmut} replicating cells (Figures S1C and S1D). This would contribute to the previous reported DNA damage checkpoint activation and G2/M arrest observed upon SET8 stabilization (Centore et al. 2010; Oda et al. 2010; Tardat et al. 2010). In conclusion, our results demonstrate that the switch from H4K20me0 to H4K20me1 induced by SET8 stabilization during S-phase is sufficient to inhibit HR nuclear foci formation.

SET8 is an inhibitor of homologous recombination. The results described above suggest that sustaining SET8 activity impairs homologous recombination (HR) during S-phase. This hypothesis is also supported by a previous report showing that the overexpression of SET8 reduces the loading of BRCA1 and RAD51 on chromatin upon ionizing radiation (Pellegrino et al. 2017). To demonstrate that SET8 can function indeed as an inhibitor of homologous recombination, control (-TET) and SET8^{PIPmut}

expressing cells (+TET) were treated with camptothecin (CPT) for 2 hours to induce DNA damage and then the number of RAD51, BRCA1 and 53BP1 nuclear foci were examined by immunofluorescence. Camptothecin (CPT) is a Topoisomerase-I poison that promotes DNA breakage at replication forks and that are mainly repaired by HR in U2OS cells (Han et al. 2022). Accordingly, CPT led to the activation of the DNA damage checkpoint kinase ATM (Figure S2A) followed by the focal accumulation of RAD51, BRCA1 and 53PB1 in a dose-dependent manner in control cells (Figures 3A and 3B). In contrast, although ATM is still normally activated in tetracycline-treated cells upon CPT treatment (Figure S2A), FLAG-SET8^{PIPmut} expression prevented the focal accumulation of RAD51 and BRCA1, but not of 53BP1 that was even increased (Figures 3A and 3B). Importantly, RPA foci formation on DNA lesions was observed in both control and SET8^{PIPmut} expressing cells upon CPT treatment (Figure S2B), indicating that the loss of RAD51 foci formation was not indirectly caused by defects in RPA loading at DNA breaks. Consistent with the accumulation of 53BP1 instead of BRCA1, we also observed the specific phosphorylation of DNA-PKcs at Serine 2056 upon CPT in FLAG-SET8^{PIPmut} expressing cells (Figure S2A), thereby suggesting the activation of NHEJ pathway rather than the HR pathway.

To further corroborate these results, the efficiency of HR upon SET8 expression was assessed using a DR-GFP reporter-based HR system stably integrated into the genome of U2OS cells. This DR-GFP system consists of two unique inactive copies of the GFP gene integrated at the same loci. The first GFP copy (SceGFP) contains the I-SceI restriction site with an in-frame stop codon and the second copy (secGFP) harbors truncations at both ends. After cleavage within SceGFP copy by I-SceI, mostly HR uses secGFP as a template to restore a functional GFP gene. Then, GFP fluorescence can be detected using flow cytometry as an indirect measure of HR

efficiency. DR-GFP cells were first transduced with retroviral vectors encoding either FLAG-SET8^{WT}, FLAG-SET8^{PIPmut} or the inactive FLAG-SET8$^{PIPmut+SETmut}$ protein and then transfected with a plasmid expressing Sce1. As shown in figure 3B and consistent with defects in HR foci formation in absence (Figure 2) as well as in presence of exogenous DNA damage (Figure 3A), the expression of FLAG-SET8^{PIPmut} strongly reduced the efficiency of HR in a manner depending on its methyltransferase activity (figure 3C). As expected, however, the HR efficiency was only slightly reduced in cells expressing FLAG-SET8^{WT} (Figure 3C) that was still highly degraded during S and G2 phases when HR is active (Tardat et al. 2010). Taken together, these results demonstrate that the proper activation of homologous recombination during S/G2 phases requires the PCNA-coupled degradation of SET8 in order to avoid the HR inhibition mediated by the SET8-induced lysine methylation on chromatin.

The anti-recombinogenic functions of SET8 depends on the recruitment of 53BP1. BRCA1 was previously shown to displace 53BP1 from chromatin in the vicinity of DSBs, thus countering the resection barrier and promoting RAD51 loading and HR during S and G2 phases (Chapman et al. 2012). Accordingly, the loss of 53BP1 can largely restore HR in BRCA1-deficient mice by rescuing RAD51 foci formation (Bunting et al. 2010). Given the role of SET8-induced H4K20me1 on the recruitment of 53BP1, we therefore reasoned that the anti-recombinogenic functions of SET8 might depend on 53BP1. To test this hypothesis, we examined the levels of RAD51 foci formation in control and FLAG-SET8^{PIPmut} expressing cells depleted or not for 53BP1. Two days after two rounds of siRNA transfection to efficiently deplete 53BP1, cells were treated with tetracycline to induce FLAG-SET8^{PIPmut} expression and then pulse-labelled with EdU before to evaluate RAD51, BRCA1 and BARD1 nuclear foci formation by

immunofluorescence. The levels of FLAG-SET8^{PIPmut} expression and the depletion of 53BP1 were verified by immunoblotting (Figure S3). As shown in Figure 4A, while 53BP1 depletion slightly increased the number of RAD51 foci in untreated control cells, the formation of RAD51 foci was fully rescued in FLAG-SET8^{PIPmut} expressing cells depleted for 53BP1(Figure 4A). Similarly, 53BP1 depletion was sufficient to fully rescue BRCA1 focal accumulation in FLAG-SET8^{PIPmut} expressing cells (Figure 4B), although the levels of BARD1 nuclear foci were only slightly rescued (Figure 4C). We conclude from these experiments that the inhibition of BRCA1 signaling upon SET8 activity and the subsequent loss of RAD51 foci depends on 53BP1 and its recruitment on replicated chromatin.

The SET8-induced switch from BRCA1/BARD1 to 53BP1 recruitment on replicated chromatin is independent of SUV4-20H activity on H4K20me1. A previous report has proposed that the inverse relationship between 53BP1 recruitment and the maturation of replicated chromatin is triggered by the replication-coupled dilution of H4K20me2, which is a high-affinity binding site for 53BP1 (Michelena et al. 2021; Pellegrino et al. 2017). Hence, we asked whether a conversion of H4K20me1 to H4K20me2 by SUV4-20Hs was necessary for the accumulation of 53BP1 on replicated chromatin upon SET8 stabilization or whether the switch from H4K20me to H4K20me1 might be sufficient on its own since 53BP1 can also bind to H4K20me1. To discriminate between the two possibilities, we examined whether the pharmacological inhibition of SUV4-20Hs prevented 53BP1 binding and thus restored BRCA1 and RAD51 foci formation in FLAG-SET8^{PIPmut} replicating cells. To this end, Tet-inducible FLAG-SET8^{PIPmut} cells were co-treated with tetracycline and the validated SUV4-20H-inhibitor A196. After EdU-labelling of replicating cells, the

formation of 53BP1 and HR nuclear foci were examined by immunofluorescence as described above. The treatment with 10μM of A196 was sufficient to inhibit *de novo* SUV4-20H activity and prevents the potential conversion of H4K20me1 to higher H4K20me states upon FLAG-SET8^{PIPmut} expression (Figure S4A). As shown in Figure 5, the focal accumulation of 53BP1 and the concomitant loss of BARD1, BRCA1 and RAD51 nuclear foci during S phase were identical between FLAG-SET8^{PIPmut} expressing cells, whether they were treated or not with A196 (Figures 5A-5D). Similar results were obtained with cells treated with A196 for 5 days and that displayed a complete loss of H4K20me2/me3 marks before tetracycline treatment to induce FLAG-SET8^{PIPmut} expression (Figures S5). Taken together, these results show that 53BP1 binding to post-replicated chromatin and the following HR inhibition upon SET8 stabilization are actually independent of SUV4-20Hs activity and the conversion of H4K20me1 to higher H4K20me states.

SET8-induced 53BP1 focal accumulation requires the recruitment of RNF168 on replicated chromatin. By inducing the ubiquitination of histones and others factors, the ubiquitin ligase RNF168 has been reported to be an upstream regulator of 53BP1 that is critical for HR defects caused by BRCA1 deficiency (Krais et al. 2021 ; Zong et al. 2019 ; Zong et al. 2015). Interestingly, SET8 directly interact with RNF168 and promotes RNF168 ubiquitin activity towards histone H2A (Dulev et al. 2020; Lu et al. 2021), thereby raising the possibility that 53BP1 focal accumulation induced by SET8 stabilization might depend on RNF168. Consistent with this possibility, FLAG-SET8^{PIPmut} expressing cells displayed RNF168 focal accumulation that significantly overlapped with 53BP1 (Figures 6A and supplementary Figure S6A). This was accompanied by an apparent enrichment of ubiquitinated chromatin proteins as

observed by the detection of 53BP1 foci positive for the anti-ubiquitinylated proteins antibody FK2 (Figure 6B). As observed for 53BP1, the focal accumulation of RNF168 during DNA replication was also enhanced in presence of DNA lesions in FLAG-SET8^{PIPmut} cells treated with camptothecin (Figure S6B). However, the focal accumulation of RNF168 was not reduced upon 53BP1 depletion (Figure S6C) or when SUV4-20H enzymes were inhibited (Figure S6D). These results indicate that the recruitment of RNF168 on replicated chromatin upon SET8 stabilization occurs independently of 53BP1 and the conversion of H4K20me1 to higher H4K20me states. Conversely, to determine whether the recruitment of RNF168 in response to SET8 stabilization contributes to the focal accumulation of 53BP1 on replicated chromatin and the inhibition of homologous recombination (HR), we examined by immunofluorescence the levels of 53BP1, BRCA1 and RAD51 nuclear foci formation in control and FLAG-SET8^{PIPmut} expressing previously depleted or not with RNF168 by siRNA. The depletion of RNF168 and the expression of FLAG-SET8^{PIPmut} were verified by immunoblotting (Figure S6E). As shown in Figures 6C and 6D, depletion of RNF168 significantly decreased 5BP1 focal accumulation in FLAG-SET8^{PIPmut} replicating cells, thereby suggesting that RNF168 contributes indeed to the untimely accumulation of 53BP1 orchestrated by SET8 stabilization on replicated chromatin. However, although 53BP1 focal accumulation was strongly reduced upon RNF168 depletion, BRCA1 and RAD51 foci formation was not rescued (Figures 6C and 6E). Instead, we even observed a decrease in HR foci in control cells depleted for RNF168 compared to siRNA control cells (Figure 6E). This was consistent with previous reports showing that RNF168 activity contributes to BRCA1 recruitment and functions, likely via the ability of BARD1 to interact with histone H2A ubiquitination (Becker et al. 2021; Krais et al. 2021, 168). Altogether, our results suggest a scenario where SET8 stabilization

on replicated chromatin subsequently favors RNF168 recruitment and protein ubiquitination that, in parallel to the conversion of H4K20me0 to H4K20me1, lead to a post-replicated chromatin organization attractive for 53BP1 but refractory to BRCA1dependent HR.

The restriction of BRCA1 chromatin binding outside of S/G2 phases depends on SET8. In order to avoid genetic aberrations, the functions of BRCA1 in homologous recombination must be suppressed from G1 phase to early S-phase, when only homologous chromosomes are available (Hustedt et Durocher 2017). Based on the findings described above and that chromatin is enriched in H4K20me1 during G1 and early-S phases, we reasoned that the restriction of BRCA1 chromatin recruitment outside of S/G2 phases might depend on SET8 methyltransferase activity. To explore further this hypothesis, U2OS cells were synchronized at G1/S transition by double thymidine block, transfected with control or SET8 siRNA for 12 hours, then released from the G1/S transition before FACS analysis of cell-cycle progression. Both control and SET8 siRNA-treated cells were able to progress similarly through S-phase, then exited from mitosis 15 hours after release with, however, high levels of H4K20me0 instead of H4K20me1 in SET8 depleted cells (Supplementary Figure S7). At 15 hours post release and compared to control cells, immunoblots after biochemical fractionation showed the loss of BRCA1 in S1 fraction of cytoplasmic components and its concomitant enrichment in P3 chromatin-enriched fraction of SET8 depleted cells harboring H4K20me0. In contrast, the chromatin binding of 53BP1 was slightly but significantly decreased, as observed by the lower levels of 53BP1 in P3 fraction and its concomitant increase in S2 fraction with soluble nuclear components (Figure 7A). In a previous study, we showed that G1/S synchronized cells depleted for SET8

started to accumulate DNA breaks as they progressed in G1 phase after a first mitosis without SET8 (Shoaib et al. 2018). In agreement with this, FACS analysis showed that synchronized control cells continued to progress through the cell cycle, whereas an accumulation at G1/S transition was observed for SET8 depleted cells associated with improper BRCA1 chromatin enrichment (Figures 7A and 7B). Furthermore, EdU pulse labelling followed by immunofluorescence showed that this G1/S arrest was accompanied by a focal accumulation for BRCA1, but not for 53BP1, in most of SET8 depleted cells (Figure 7C). In contrast, control G1 cells negative for EdU only displayed rare BRCA1 foci, which emerged when control cells entered and progressed into S phase as expected (Figure 7C). Altogether, these results showed that the loss of SET8 and the following absence of conversion of H4K20me0 to H4K20me1 at the end of DNA replication impaired 53BP1 chromatin regulation and to induce conversely an inaccurate focal and chromatin accumulation of BRCA1 in the following G1 phase of daughter cells.

G1/S arrest upon SET8 depletion depends on BRCA1. Since the inaccurate BRCA1 foci formation outside of S-phase could have deleterious cellular effects (Callen et al. 2020), we wondered whether the G1/S transition defects upon SET8 depletion might be actually caused by BRCA1. To address this question, U2OS cells were first transduced with retroviral vectors expressing shRNA control or shRNA SET8 and the following days transduced cells were transfected with an irrelevant control siRNA or a siRNA directed against BRCA1. Two days after treatment, cells were pulse-labeled with BrdU and DNA replication progression were analyzed by FACS. Whereas BRCA1 siRNA treatment by its own did not affect S phase entry as measured by FACS analysis, depletion of BRCA1 was sufficient to partially restore BrdU

incorporation and normal S-phase progression in SET8 depleted cells (Figure 7D). These results suggest that the G1/S arrest upon SET8 depletion was triggered by the inaccurate binding of BRCA1 on chromatin. Taken together, our results demonstrate the importance of the timely *de novo* SET8-induced H4K20 mono-methylation in the regulatory cell-cycle inhibition of BRCA1 signaling in absence of exogenous DNA damage, an essential mechanism for the maintenance of genome integrity during normal cell proliferation.

DISCUSSION

While our knowledge of the mechanisms that activate BRCA1-mediated HR pathways upon exogenous sources of DNA damage is extensive, the mechanisms that regulate BRCA1 activity upon unchallenged conditions of cell-cycle progression still remains poorly understood. Yet, BRCA1-mediated HR signaling is required for repair of spontaneous double-stranded breaks (DSBs) that arise during DNA replication, a function that has to be tightly controlled to ensure proper cell cycle progression and avoid pathological situations such as in breast or ovarian carcinomas (Tarsounas and Sung 2020). In this study, we demonstrate that the recruitment of SET8 and the subsequent single switch from K20me0 to K20me1 is a natural inhibitory signal of BRCA1 functions in homologous recombination during the cell cycle. Indeed, in absence of exogenous source of DNA damage, the binding of SET8 on newly replicated chromatin in cooperation with the RNF168 ubiquitin ligase are sufficient to turn off the HR functions of BRCA1 by promoting the chromatin recruitment of 53BP1, independently of the H4K20me2/me3 states induced by SUV4-20H enzymes. Conversely, the lack of SET8 and the following impairment in H4K20me1 restoration

after DNA replication led to an inaccurate chromatin accumulation of BRCA1 at the exit of mitosis, contributing to defects in 53BP1 chromatin binding and in the entry of the following S-phase. Taken together, these results clarify the mechanisms by which de novo SET8 and H4K20 mono-methylation impact on DNA repair pathways choice and establish the concerted activities of SET8 and RNF168 on chromatin as the key inhibitory lock of BRCA1 recombinogenic functions that must be specifically lifted during S and G2 phases and properly re-established thereafter to ensure proper regulation of HR during the cell cycle.

Our results are consistent with a previous study showing that the overexpression of SET8 reduces BRCA1 and RAD51 foci formation and inversely promotes 53BP1 focal accumulation on damaged chromatin upon ionizing radiation (Pellegrino et al. 2017). However, upon ionizing radiation, the conversion of H4K20me1 to H4K20me2 appeared to function downstream of SET8 in 53BP1 chromatin recruitment at DNA breaks (Pellegrino et al. 2017). Our results do not favor this hypothesis in unchallenging cellular conditions, where the recruitment of 53BP1 on post-replicative chromatin appear independent from the activity of SUV420H1 and SUV4-20H2 enzymes responsible for the conversion of H4K20me1 to higher H4K20me states. Strikingly, several studies have reported conflicting results regarding the H4K20me states and the H4K20 enzymes that dictate the recruitment of 53BP1 on damaged chromatin. Whereas the decrease in H4K20me2/me3 upon the SUV4-20H inhibitor A196 reduces 53BP1 foci formation upon ionizing radiation in cancer cells (Bromberg et al. 2017)), the loss of these enzymes and the absence of H4K20me2/3 only induced a slight delay on 53BP1 focal accumulation at DNA breaks in mouse embryonic fibroblasts (Schotta et al. 2008). We believe that this apparent discrepancy ultimately reflects the disparate *in vivo* affinity of 53BP1 for the different

H4K20me states. This likely translates into different modes of 53BP1 recruitment depending on the level and nature of DNA damage sustained, the chromatin epigenetic landscape, and the phases of the cell cycle. Thus, our results demonstrate that the 53BP1 recruitment to chromatin in the absence of exogenous DNA damage is linked to SET8's dual functions: (i) the ability of SET8-induced H4K20me1 to evict H4K20me0 readers and their associated HR factors notably BRCA1 and (ii) the ability of SET8 to create efficient 53BP1 binding sites along the genome via the switch from H4K20me0 to H4K20me1 and by promoting RNF168-mediated chromatin ubiquitination.

A potential mechanism by which SET8 could stimulate RNF168 activity is suggested by two recent studies showing that SET8 directly interacts with RNF168 and that this interaction is important for SET8 recruitment to DNA damage while enhancing RNF168 ubiquitin activity on chromatin proteins (Dulev et al. 2020, 8; Lu et al. 2021). Noted of, RNF168 activity is finely regulated notably by two other E3 ubiquitin ligases, TRIP12 and UBR5, which prevent excessive chromatin ubiquitination in the vicinity of DNA damage sites (Gudjonsson et al. 2012). In addition, several de-ubiquitinases (DUBs) and ubiquitin-specific proteases (USPs) have also been found to counterbalance the chromatin ubiquitination induced by RNF168 (Kelliher et al. 2022), thereby contributing to regulate properly the activity of ubiquitination-dependent DNA damage response pathway factors, such as 53BP1 and BRCA1. In this regard, our iPOND experiments showed that, in addition to BRCA1, the binding of SET8 on newly replicated chromatin might trigger the eviction of several proteins involved in the inhibition of histone ubiquitination, such as OTUB1, TRIP12 and USP3 (Figure 1E), which could also indirectly explain the stimulation of protein ubiquitination upon SET8 binding on post-replicated chromatin.

It is well established that HR defects in BRCA1-deficient cells can be compensated by the inactivation of 53BP1 (Bunting et al. 2010). Furthermore, depending on the mechanism of BRCA1 inactivation, 53BP1 exerts its role of inhibiting either DNA resection step or the deposition of RAD51 on DNA post-resection (Callen et al. 2020). Since H4K20me0 is a post-replicative mark during S-phase and incompatible with 53BP1 recruitment, it has been suggested a post-replicative marking model where H4K20me0 and its recognition by BARD1 and TONSL tips the balance of repair in favor of BRCA1 and HR factors (Nakamura et al. 2019, 0; Saredi et al. 2016, 0). Yet, the full restoration of BRCA1 and RAD51 focal accumulation, but not of BARD1, can be compensated by the depletion of 53BP1 despite the absence of H4K20me0 (Figure 4). Therefore, our results suggest a more complex model where BRCA1 is also recruited on replicated chromatin independently of the recognition of H4K20me0 by BARD1 and that SET8-induced 53BP1 chromatin binding also prevents the BRCA1 recruitment mechanism independent from H4K20me0. This could be related to the ability of BRCA1 to form distinct protein complexes through the association of different partners (Savage and Harkin 2015). A mutual, but not exclusive, possibility is that the recruitment of RNF168 induced by SET8 contribute to restore nuclear BRCA1 and RAD51 foci in absence of 53BP1. Indeed, it has been recently shown that RNF168 interacts with PALB2, which favors the loading of RAD51 on DNA when BRCA1 HR functions are compromised (Zong et al. 2019).

Another important finding of our study is that the absence of SET8 and the restoration of H4K20me1 signal at the exit of mitosis leads to an excessive binding of BRCA1 on chromatin and its focal accumulation, whereas we observed the reverse effect for 53BP1 (Figure 7). Since the loss of SETD8 activity leads to chromatin relaxation and progressive DNA damage after exit of mitosis (Shoaib et al. 2018), we

believe that the untimely BRCA1 focal accumulation in G1 cells are related to these chromatin alterations. The formation of BRCA1 foci outside of S/G2 phase is not unprecedented, since 53BP1 depletion resulted in ectopic BRCA1 foci upon ionizing radiation in G1 cells (Escribano-Díaz et al., 2013). However, 53BP1 depletion is not sufficient to induce the recruitment of the PALB2/BRCA2/RAD51 complex in G1 cells (Orthwein et al. 2015), which is consistent with the lack of HR activity despite the focal accumulation of BRCA1 in these cells. Similarly, the switch from 53BP1 to BRCA1 upon SET8 depletion is not a sufficient event to activate HR in G1 cells. Recently, it has been shown that BRCA1 foci can been found at damaged centromeric regions in G1 cells in a manner depending on the histone variant CENP-A and histone H3K4 di-methylation (Yilmaz et al. 2021), suggesting that the chromatin recruitment of BRCA1 can occur in specialized chromatin regions of the genome independently of DNA replication. Although further experiments are required to unravel these mechanisms, it is tempting to imagine that the local and timing regulation of SET8 and H4K20me states during the cell cycle might play a key role in preventing BRCA1 chromatin spreading outside of centromeric regions. This would explain the G1-S transition defects observed after one round of cell division without SET8 and that can be partially rescued by BRCA1 depletion (Figure 7). This is also reminiscent of a previous observation showing that targeting RAD51 by siRNA partially restored S-phase progression in asynchronous SET8 depleted cells (Jørgensen et al. 2007). Thus, while BRCA1 mediated homologous recombination functions are essential to deal with DNA damage naturally occurring in unchallenged replication conditions, our results indicate that BRCA1 activation before or too early during S-phase upon loss of SET8 epigenetic functions is incompatible with proper DNA replication process.

Clinically, SET8 has been found upregulated in several types of cancers and often associated with poor prognosis (Liao et al. 2018 ; Milite et al. 2016 ; Yang et al. 2021). The higher-level of SET8 in cancer cells could be due to multiple mechanisms, including DNA copy-number gains, changes in gene expression or enhanced protein stability (Hernández-Reyes et al. 2022; Veo et al. 2019 ; Veschi et al. 2017). To date, however, the benefit of high levels of SET8 on cancer cell development and resistance is far from understood. Given the importance of BRCA1 deficiency in tumorigenesis and our novel findings regarding the inhibitory role of SET8 on BRCA1 during the cell cycle, it will be interesting in near future to explore whether SET8 might contribute to the reduction of functional BRCA1. Notably, this issue appears important in tumors where BRCA1 dysfunctions cannot be easily explained by mutations or loss of expression as observed in certain subtypes of sporadic breast and ovarian cancers where SET8 is found upregulated.

EXPERIMENTAL PROCEDURES

Cell culture and chemical drugs

HEK293T, U2OS, DR-GFP, U2OS Tet-On cell lines were cultured at 37°C in Dulbecco's Modified Eagle Medium (DMEM) with Glutamax (Gibco) and supplemented with 10% Fetal Bovine Serum (FCS), 1% antibiotics (Gibco) and 1% Sodium Pyruvate (Gibco). Expression of the different FLAG-SET8 proteins in U2OS cells were induced by the addition of 2 µg/ml of tetracyclin (TET) (Sigma-Aldrich) into cell culture medium. G1/S synchronization was performed by double thymidine block as described previously. Alternatively, confluent cells arrested in G1 were seeded at low density in presence of 2.5 mM Thymidine (Sigma-Aldrich) for 24 hours. Release of cells from G1/S block was performed by three cycles of washes with PBS then fresh medium for 5 minutes at 37°C. The SUV4-20H inhibitor A196 (Sigma-Aldrich) was used at the concentration of 10 µM. Camptothecin (C9911, Sigma-Aldrich) was used to induce replicative stress and DNA breaks during S-phase.

RNA interference experiments

One day after seeding 10^6 U2OS cells in 6-well plate, small interfering RNAs (siRNA, 20µM) were delivered using Lipofectamine® RNAi-MAX Reagent (Invitrogen) according to the supplier's instructions. Briefly, transfection mixture containing 300 µl Optimem (Gibco), siRNA and Lipofectamine® RNAi-MAX Reagent was added to each well containing 1 ml of culture medium for 6 to 8 hours at 37°C before washing the cells with PBS and culturing them in fresh medium. SET8 siRNA sequence was provided and validated by Cell Signaling (#1307). The other validated siRNA sequences were

provided by Sigma-Aldrich (MISSION® esiRNA): Control (EHURLUC, EHUFLUC, EHUGFP), TP53BP1 (EHU156121), RAD51 (EHU045521), BRCA1 (EHU096311), RNF168 (EHU011891). Retroviral pSIREN vectors expressing shRNA sequences directed against SET8 or Luciferase (Control) were described previously (Tardat et al. 2007). Briefly, retroviral particles were collected two days after two rounds (at 24h interval) of plasmid transfection into HEK293T cells. After filtration, retroviral particles were directly added to U2OS cells in the presence of polybrene (8 µg/ml, Sigma-Aldrich). Twenty-four hours after infection, shRNA expressing cells were selected with puromycin (1 µg/ml).

Cell-Cycle analysis by Flow Cytometry

Cells were incubated with BrdU (50 µg/ml, Sigma-Aldrich) for 90 minutes before fixation in ice-cold 70% ethanol. After incubation for 30 minutes with solution containing 2N HCl and 0.5% Triton X-100 under gentle agitation, cells were washed with Borax buffer (pH8.5) and then sequentially incubated in blocking solution (PBS, 0,5% Tween 20,1% BSA) containing anti-BrdU primary antibody (1/100, BD Biosciences) and anti-mouse secondary antibody coupled to FITC (1/300, Sigma-Aldrich) for 2 hours each. Total DNA was labeled with 2 µg/ml of 7-AAD (7-amino-actinomycin D, Sigma-Aldrich) diluted in PBS containing 100 µg/ml of RNAse A (Sigma -Aldrich). FACS analysis was carried out with Gallios flow cytometer (Beckman Coulter) using the Kaluza Acquisition software (Beckman Coulter). Cell cycle profiles were analyzed using FlowJo software (BD Biosciences). the data were presented with mean ± s.e.m. from at least three independent experiments. Statistical significance was evaluated by an unpaired t-test. ns : p-value > 0.05 ; * : p-value < 0.05 ; ** p-value < 0.01 ; *** : p-value < 0.001.

Homologous recombination (HR) assays

The HR assays were performed using the U2OS DR-GFP cell line (ATCC) that allows to monitor homologous recombination efficiency through the detection of GFP positive cells via flow cytometry. One day after infection with retroviral empty pBABE vector or expressing FLAG-SET8^{WT}, FLAG-Set8^{PIPmut} or FLAG-Set8$^{PIPmut+SETmut}$, cells were transfected with 5 ug of plasmid encoding the I-SceI endonuclease using JetPEI reagent and following manufacturer's instructions. Cells were then collected two days later, fixed in 1% Formaldehyde for 15 minutes and then permeabilized for 1h at 4 °C. After one hour incubation with 2 µg/ml of 7-AAD, the measure of DNA content and the percentage of GFP positive cells were carried out with Gallios flow cytometer (Beckman Coulter) using the Kaluza Acquisition software (Beckman Coulter). FACS data were analyzed using FlowJo software (BD Biosciences). The results are presented as mean ± s.e.m. from four independent experiments with *p*-values determined with unpaired t-test.

Immunostaining and Microscopy analysis

After incubation for 20 minutes with 10 µM of EdU (Invitrogen), cells on microscope slides were treated with ice-cold PBS containing 0.25% Triton for 2 min and then fixed with 4% formaldehyde for 12 min. After permeabilization with PBS containing 0.25% Triton for 10 min, incorporated EdU was chemically conjugated to Alexa 647 fluorochrome using Click-iT Plus EdU Cell Proliferation Kit (Invitrogen). After PBS washing, samples were incubated for one hour in a blocking solution (PBS, 0.1% Tween 20, 5%BSA), before adding the primary antibody for an overnight incubation in a humid chamber at 4°C. After washing in PBS containing 0,1% Tween 20, cells were incubated with secondary antibodies for 2 hours at RT in a humid chamber and DNA

was counterstained with 0.1 µg/ml of DAPI (DNA intercalator, 4',6-Diamidino-2-Phenylindole, D1306, Invitrogen). Coverslips were mounted with ProLong Diamond Antifade (Invitrogen). The following primary antibodies used were anti RPA70 (1:100, #2267, Cell Signaling), anti-53PB1 (1:500, Cell Signaling and 1:1000, Millipore), anti-RNF168 (1:100, GTX129617, Genetex), anti-RAD51 (1:500, PC130, Millipore), anti-gH2A.X (1:1000, Millipore), anti-FK2 (&:250, Millipore), anti-BRCA1 (1:500, , sc-6954, Santa-cruz), anti BARD1 (1:500, PLA0074, Sigma). The secondary antibodies used were anti-Rabbit-Alexa Fluor 488 (1/500, Thermo Fisher Scientific) and anti-Mouse-Cy3 (1/500, Thermo Fisher Scientific). Slides were analyzed using Zeiss Axio Imager M2 upright microscope (Zeiss) equipped with an Apochromat 63X objective (NA 1.4, immersion oil). Images were acquired using an ORCA-Flash4.0 LT+ Digital CMOS camera (C1140-42U30, Hamamatsu) controlled by Zen acquisition software (Zeiss). Images were prepared using Zen software and nuclear foci were quantified using CellProfiler™ software. Representative images were prepared using Photoshop software (Adobe). Statistical significance was evaluated by an unpaired t-test. ns : p-value > 0.05 ; * : p-value < 0.05 ; ** p-value < 0.01 ; *** : p-value < 0.001.

Protein extraction, immunoblot analysis and small-scale fractionation.

Cells were lysed at 95°C for 10 minutes in 2X SDS Sample Buffer (100 mM Tris-HCl pH6.8, 20% Glycerol, 2% SDS 2%, 1 mM DTT, 5% β-mercaptoethanol). Proteins samples were separated on polyacrylamide gel under denaturing conditions (SDS-PAGE) and transferred to nitrocellulose or PVDF membranes following the primary antibodies used. Before incubation with primary and secondary antibodies, membranes were saturated in a solution of TBS containing 0.2% Tween 20 and 5% w/v of dried milk for 16 hours at 4°C. For immunoblots analysis the following antibodies

were used : anti-H4K20me0 (1:1000, Abcam), anti-histone H3 (1:5000, Cell Signaling), anti-histone H4 (1:1000, Cell Signaling), anti-H4K20me states (1:1000, cell Signaling), anti-SET8 1:1000 , Cell Signaling), anti-53BP1 (1:1000, cell Signaling), anti-BRCA1 (1:1000, cell Signaling), anti-ATM and anti-pS1981-ATM (1:1000, cell Signaling), anti-DNA-PK unphosphorylated (1:1000, Millipore) and phosphorylated at S2056 (1:1000, Cell Signaling), anti-RNF168 (1:1000 Genetex), anti-FLAG (1:1000, Sigma) and anti-Tubulin (1:1000, Sigma). The following secondary antibodies were used anti-rabbit (1/10000, Cell Signaling) and anti-mouse (1 /10000, Cell Signaling). Protein bands were visualized on X-ray film by electro-chemiluminescence (Immobilon Western HRP Substrate, WBKLS0500, Millipore).

For the isolation of chromatin-enriched proteins, small-scale biochemical fractionation was prepared with 10^7 cells as described previously (Tardat et al. 2010). Briefly, cells were incubated with Buffer A (10 mM Hepes pH 7.9, 10 mM KCl, 1.5 mM MgCl2, 350 mM Sucrose, 0.1% Triton, 10% Glycerol and protease inhibitors (Roche)) for 5 minutes on ice in order to solubilize cytoplasmic proteins. After centrifugation, supernatant containing cytoplasmic proteins was collected and nuclei pellet was lysed in Buffer B (3 mM EDTA, 0.2 mM EGTA) for 30 minutes on ice with regular agitation. After centrifugation, nuclear soluble proteins were collected (supernatant) and pellet proteins containing the chromatin-enriched fraction was solubilized in 2X SDS Sample buffer.

i-POND assay

After incubation with tetracycline (TET) to induce FLAG-Set8^{PIPmut} expression and eventually G1/S synchronization with thymidine before released into S-phase, 10^8 cells were incubated with 10 µM EdU for 20 minutes to label ongoing replication forks

before fixation with 2% formaldehyde for 20 minutes at a concentration of $2x10^6$ cells/ml. Formaldehyde quenching was done by adding 125 mM Glycine for 5 minutes. Cells were then permeabilized for 10 minutes on ice with PBS containing 0.25% Triton. Samples were then incubated in PBS solution containing 2 mM CUSO4 and 2 mM BTTP for 60 min at the concentration of $20x10^6$ cells/ml, before EdU conjugation to Biotin (Click reaction) by adding 10 mM Sodium-L-Ascorbate, 20 µM Biotin-TEG (Sigma-Aldrich) for 30 minutes on a rotating wheel (Click reaction). For "No Click" condition, Biotin-TEG was replaced by DMSO. Cells were then lysed in LB3JD Lysis Buffer (10 mM Hepes, pH 8, 100 mM NaCl, 500 mM EDTA pH 8, 100 mM EGTA pH 8, 0.2% SDS, 0.1% N-Lauroylsarcosine supplemented with 1mM PMSF and protease inhibitors (Roche)) at the concentration of $4x10^7$ cells/ml. Fixed chromatin was sheared using Bioruptor Pico (Diagenode) for 15 min or using the EpiShearTM Probe Sonicator probe. Samples were clarified by centrifugation at 15,000 rpm for 10 minutes. Aliquots corresponding to 1/100 of the final volume were saved for immunoblots and chromatin fragmentation analysis. 50 µl of streptavidin magnetic beads (Ademtech) were added to the EdU/Biotin-TEG-labeled chromatin and samples were incubated for 16-20h on a rotating wheel at 4°C in the dark. Beads were washed with LB3JD Lysis Buffer, then with 500 mM NaCl and twice again with LB3JD Lysis Buffer. Finally, purified DNA/protein complexes were eluted from beads and denatured with 50-70 µl of denaturation buffer (125 mM Tris-HCl pH6.8, 5% Glycerol, 2% SDS, 100 mM DTT, 2% β- mercaptoethanol) by heating at 95° C for 30 minutes with vigorous shaking. In parallel, one aliquot of total extract was denatured under the same conditions after adding of denaturation buffer at a 1:1 ratio. To verify chromatin fragmentation, the second aliquot was two times diluted in SDS buffer (50 mM Tris-HCl pH8, 1 mM EDTA pH8, 2% SDS) then heated to 65°C overnight with vigorous

shacking. Aliquot was diluted in TE Buffer (50 mM Tris-HCl pH8, 100 mM NaCl, 1 mM EDTA) and treated with RNAse A (200 µg/ml, 45 min at 37°C) and with proteinase K (20 µg/ml, 30 min. at 37°C and 30 min. at 55°C). DNA was then purified with phenol/chloroform (Sigma-Aldrich) followed by ethanol/sodium acetate precipitation. DNA was analyzed on 2% agarose gel. For iPOND samples analysis by mass spectrometry, $2x10^9$ cells per condition were used.

Mass Spectrometry Analysis

For iPOND followed by MS, protein extracts were resolved by SDS-PAGE (10 %) and detected with Coomasie-brillant blue staining. Electrophoretic lanes were cut in five fractions. Gel pieces (2 × 2 mm) proceeded as previously described (Shevchenko et al. 2006). Briefly, gel pieces were washed by water, dehydrated by 50% acetonitrile (ACN) in 50mM NH_4HCO_3, then 100% ACN and dried. After DDT reduction and iodoacetamid alkylation, gel pieces were re-swollen in a 0.1µg/µl trypsin (Promega) solution ($NH_4HCO_3$100mM, $CaCl_2$ 0.5M, 1% proteasmax). Resulting peptides were trapped and desalted on C18 Zip-Tips (Agilent) and concentrated via speed-vaccum. For LC-MS/MS, the peptide mixtures were dissolved in 10 µl 0.1% formic acid (FA) and loaded on an Ekspert 425 nanoLC system (Sciex) equipped with a C18 column (Discovery BIO Wide Pore, 3um, 0.5x10cm, Supelco). The mobile phases were solvent A (water, 0.1% FA) and B (acetonitrile, 0.1% FA). Injection was performed with 95% solvent A at a flow rate of 5µl/min. The peptides were separated with the following gradient: 5% to 40% B in 100min, 40% to 80% B in 5min and the separation was monitored on-line on a TripleTOF 5600 mass spectrometer (Sciex). The total ion chromatogram (TIC) acquisition was made in information dependent acquisition (IDA) mode using Analyst TF v.1.6 software (Sciex). Each cycle consisted of a TOF-MS

spectrum acquisition for 250 msec (350-1600Da), followed by acquisition of up to 30MS/MS spectra (75 msec each, mass range 100-1600Da), of MS peaks above intensity 400 taking 2.5 sec total full cycle. Target ions were excluded from the scan for 15s after being detected. The IDA advanced 'rolling collision energy (CE)' option was employed to automatically ramp up the CE value in the collision cell as the m/z value was increased. Protein identification was then performed by the ProteinPilot software v.5.0 (Sciex). From each MS2 spectrum, the Paragon algorithm (Shilov et al. 2007) was used to searched Uniprot/Swissprot database with the following parameters: trypsin specificity, Cys-carbamidomethylation and search effort set to rapid. This calculates a confidence percentage (FRD>0.01) that reflects the probability that the hit is a false positive, meaning that at 99% confidence level (unused score>1.2), there is a false positive identification chance of about 1%. After database searching, only proteins identified with a confidence score (FDR<0.01) and a total protein score >1.0 were retained according to the analysis with ProteinPilot (Sciex). For each protein of interest, spectral count (the number of peptides assigned to a protein in an MS/MS experiment) was determined. For variation, spectral counts were normalized on the total sum of the spectral counts per biological sample using the following equation: $SpCnormi = SpCi / \sum ni=1 SpCi$.

REFERENCES

Alabert, Constance, Teresa K. Barth, Nazaret Reverón-Gómez, Simone Sidoli, Andreas Schmidt, Ole N. Jensen, Axel Imhof, et Anja Groth. 2015. « Two Distinct Modes for Propagation of Histone PTMs across the Cell Cycle ». *Genes & Development* 29 (6): 585-90. https://doi.org/10.1101/gad.256354.114.

Aze, Antoine, Jin Chuan Zhou, Alessandro Costa, et Vincenzo Costanzo. 2013. « DNA Replication and Homologous Recombination Factors: Acting Together to Maintain Genome Stability ». *Chromosoma* 122 (5): 401-13. https://doi.org/10.1007/s00412-013-0411-3.

Beck, David B., Adam Burton, Hisanobu Oda, Céline Ziegler-Birling, Maria-Elena Torres-Padilla, et Danny Reinberg. 2012. « The Role of PR-Set7 in Replication Licensing Depends on Suv4-20h ». *Genes & Development* 26 (23): 2580-89. https://doi.org/10.1101/gad.195636.112.

Becker, Jordan R., Gillian Clifford, Clara Bonnet, Anja Groth, Marcus D. Wilson, et J. Ross Chapman. 2021. « BARD1 Reads H2A Lysine 15 Ubiquitination to Direct Homologous Recombination ». *Nature* 596 (7872): 433-37. https://doi.org/10.1038/s41586-021-03776-w.

Bhowmick, Rahul, Mads Lerdrup, Sampath Amitash Gadi, Giacomo G. Rossetti, Manika I. Singh, Ying Liu, Thanos D. Halazonetis, et Ian D. Hickson. 2022. « RAD51 Protects Human Cells from Transcription-Replication Conflicts ». *Molecular Cell* 82

(18): 3366-3381.e9. https://doi.org/10.1016/j.molcel.2022.07.010.

Botuyan, Maria Victoria, Joseph Lee, Irene M Ward, Ja-Eun Kim, James R Thompson, Junjie Chen, et Georges Mer. 2006. « Structural basis for the methylation state-specific recognition of histone H4-K20 by 53BP1 and Crb2 in DNA repair ». *Cell* 127 (7): 1361-73.

Bromberg, Kenneth D., Taylor R. H. Mitchell, Anup K. Upadhyay, Clarissa G. Jakob, Manisha A. Jhala, Kenneth M. Comess, Loren M. Lasko, et al. 2017. « The SUV4-20 Inhibitor A-196 Verifies a Role for Epigenetics in Genomic Integrity ». *Nature Chemical Biology* 13 (3): 317-24. https://doi.org/10.1038/nchembio.2282.

Brustel, Julien, Mathieu Tardat, Olivier Kirsh, Charlotte Grimaud, et Eric Julien. 2011. « Coupling Mitosis to DNA Replication: The Emerging Role of the Histone H4-Lysine 20 Methyltransferase PR-Set7 ». *Trends in Cell Biology* 21 (8): 452-60. https://doi.org/10.1016/j.tcb.2011.04.006.

Bunting, Samuel F., Elsa Callén, Nancy Wong, Hua-Tang Chen, Federica Polato, Amanda Gunn, Anne Bothmer, et al. 2010. « 53BP1 Inhibits Homologous Recombination in Brca1-Deficient Cells by Blocking Resection of DNA Breaks ». *Cell* 141 (2): 243-54. https://doi.org/10.1016/j.cell.2010.03.012.

Callen, Elsa, Dali Zong, Wei Wu, Nancy Wong, Andre Stanlie, Momoko Ishikawa, Raphael Pavani, et al. 2020. « 53BP1 Enforces Distinct Pre- and Post-Resection Blocks on Homologous Recombination ». *Molecular Cell* 77 (1): 26-38.e7.

https://doi.org/10.1016/j.molcel.2019.09.024.

Cao, Xiongwen, Yanran Chen, Bin Wu, Xiaoyun Wang, Hongjuan Xue, Lu Yu, Jie Li, et al. 2020. « Histone H4K20 Demethylation by Two HHR23 Proteins ». *Cell Reports* 30 (12): 4152-4164.e6. https://doi.org/10.1016/j.celrep.2020.03.001.

Centore, Richard C, Courtney G Havens, Amity L Manning, Ju-Mei Li, Rachel Litman Flynn, Alice Tse, Jianping Jin, Nicholas J Dyson, Johannes C Walter, et Lee Zou. 2010. « CRL4(Cdt2)-mediated destruction of the histone methyltransferase Set8 prevents premature chromatin compaction in S phase ». *Molecular Cell* 40 (1): 22-33. https://doi.org/10.1016/j.molcel.2010.09.015.

Chapman, J. Ross, Alex J. Sossick, Simon J. Boulton, et Stephen P. Jackson. 2012. « BRCA1-Associated Exclusion of 53BP1 from DNA Damage Sites Underlies Temporal Control of DNA Repair ». *Journal of Cell Science* 125 (15): 3529-34. https://doi.org/10.1242/jcs.105353.

Costanzo, Vincenzo. 2011. « Brca2, Rad51 and Mre11: Performing Balancing Acts on Replication Forks ». *DNA Repair* 10 (10): 1060-65. https://doi.org/10.1016/j.dnarep.2011.07.009.

Dulev, Stanimir, Sichun Lin, Qingquan Liu, Vildan B. Cetintas, et Nizar N. Batada. 2020. « SET8 Localization to Chromatin Flanking DNA Damage Is Dependent on RNF168 Ubiquitin Ligase ». *Cell Cycle* 19 (1): 15-23. https://doi.org/10.1080/15384101.2019.1690231.

Dungrawala, Huzefa, et David Cortez. 2015. « Purification of Proteins on Newly Synthesized DNA Using IPOND ». *Methods in Molecular Biology (Clifton, N.J.)* 1228: 123-31. https://doi.org/10.1007/978-1-4939-1680-1_10.

Feu, Sonia, Fernando Unzueta, Amaia Ercilla, Alejandro Pérez-Venteo, Montserrat Jaumot, et Neus Agell. 2022. « RAD51 Is a Druggable Target That Sustains Replication Fork Progression upon DNA Replication Stress ». *PLOS ONE* 17 (8): e0266645. https://doi.org/10.1371/journal.pone.0266645.

Fradet-Turcotte, Amélie, Marella D. Canny, Cristina Escribano-Díaz, Alexandre Orthwein, Charles C. Y. Leung, Hao Huang, Marie-Claude Landry, et al. 2013. « 53BP1 Is a Reader of the DNA-Damage-Induced H2A Lys 15 Ubiquitin Mark ». *Nature* 499 (7456): 50-54. https://doi.org/10.1038/nature12318.

Gudjonsson, Thorkell, Matthias Altmeyer, Velibor Savic, Luis Toledo, Christoffel Dinant, Merete Grøfte, Jirina Bartkova, et al. 2012. « TRIP12 and UBR5 Suppress Spreading of Chromatin Ubiquitylation at Damaged Chromosomes ». *Cell* 150 (4): 697-709. https://doi.org/10.1016/j.cell.2012.06.039.

Han, Seungmin, Kwang Suk Lim, Brody J. Blackburn, Jina Yun, Charles W. Putnam, David A. Bull, et Young-Wook Won. 2022. « The Potential of Topoisomerase Inhibitor-Based Antibody–Drug Conjugates ». *Pharmaceutics* 14 (8): 1707. https://doi.org/10.3390/pharmaceutics14081707.

Hernández-Reyes, Yeray, María Cristina Paz-Cabrera, Raimundo Freire, et Veronique A. J. Smits. 2022. « USP29 Deubiquitinates SETD8 and Regulates DNA Damage-Induced H4K20 Monomethylation and 53BP1 Focus Formation ». *Cells* 11 (16): 2492. https://doi.org/10.3390/cells11162492.

Hustedt, Nicole, et Daniel Durocher. 2017. « The Control of DNA Repair by the Cell Cycle ». *Nature Cell Biology* 19 (1): 1-9. https://doi.org/10.1038/ncb3452.

Jeggo, Penny A., et Markus Löbrich. 2015. « How Cancer Cells Hijack DNA Double-Strand Break Repair Pathways to Gain Genomic Instability ». *Biochemical Journal* 471 (1): 1-11. https://doi.org/10.1042/BJ20150582.

Jørgensen, Stine, Ingegerd Elvers, Morten Beck Trelle, Tobias Menzel, Morten Eskildsen, Ole Nørregaard Jensen, Thomas Helleday, Kristian Helin, et Claus Storgaard Sørensen. 2007. « The histone methyltransferase SET8 is required for S-phase progression ». *The Journal of Cell Biology* 179 (7): 1337-45. https://doi.org/10.1083/jcb.200706150.

Jørgensen, Stine, Gunnar Schotta, et Claus Storgaard Sørensen. 2013. « Histone H4 Lysine 20 Methylation: Key Player in Epigenetic Regulation of Genomic Integrity ». *Nucleic Acids Research* 41 (5): 2797-2806. https://doi.org/10.1093/nar/gkt012.

Kelliher, Jessica, Gargi Ghosal, et Justin Wai Chung Leung. 2022. « New Answers to the Old RIDDLE: RNF168 and the DNA Damage Response Pathway ». *The FEBS Journal* 289 (9): 2467-80. https://doi.org/10.1111/febs.15857.

Kolinjivadi, Arun Mouli, Vincenzo Sannino, Anna de Antoni, Hervé Técher, Giorgio Baldi, et Vincenzo Costanzo. 2017. « Moonlighting at Replication Forks - a New Life for Homologous Recombination Proteins BRCA1, BRCA2 and RAD51 ». *FEBS Letters* 591 (8): 1083-1100. https://doi.org/10.1002/1873-3468.12556.

Krais, John J., Yifan Wang, Pooja Patel, Jayati Basu, Andrea J. Bernhardy, et Neil Johnson. 2021. « RNF168-Mediated Localization of BARD1 Recruits the BRCA1-PALB2 Complex to DNA Damage ». *Nature Communications* 12 (1): 5016. https://doi.org/10.1038/s41467-021-25346-4.

Liao, Tian, Yuan-Jin Wang, Jia-Qian Hu, Yu Wang, Li-Tao Han, Ben Ma, Rong-Liang Shi, et al. 2018. « Histone Methyltransferase KMT5A Gene Modulates Oncogenesis and Lipid Metabolism of Papillary Thyroid Cancer in Vitro ». *Oncology Reports* 39 (5): 2185-92. https://doi.org/10.3892/or.2018.6295.

Liu, Wen, Bogdan Tanasa, Oksana V Tyurina, Tian Yuan Zhou, Reto Gassmann, Wei Ting Liu, Kenneth A Ohgi, et al. 2010. « PHF8 mediates histone H4 lysine 20 demethylation events involved in cell cycle progression ». *Nature* 466 (7305): 508-12. https://doi.org/10.1038/nature09272.

Lu, Xiaopeng, Min Xu, Qian Zhu, Jun Zhang, Ge Liu, Yantao Bao, Luo Gu, Yuan Tian, He Wen, et Wei-Guo Zhu. 2021. « RNF8-ubiquitinated KMT5A Is Required for RNF168-induced H2A Ubiquitination in Response to DNA Damage ». *The FASEB Journal* 35 (4). https://doi.org/10.1096/fj.202002234R.

Michelena, Jone, Stefania Pellegrino, Vincent Spegg, et Matthias Altmeyer. 2021. « Replicated Chromatin Curtails 53BP1 Recruitment in BRCA1-Proficient and BRCA1-Deficient Cells ». *Life Science Alliance* 4 (6): e202101023. https://doi.org/10.26508/lsa.202101023.

Milite, Ciro, Alessandra Feoli, Monica Viviano, Donatella Rescigno, Agostino Cianciulli, Amodio Luca Balzano, Antonello Mai, Sabrina Castellano, et Gianluca Sbardella. 2016. « The Emerging Role of Lysine Methyltransferase SETD8 in Human Diseases ». *Clinical Epigenetics* 8: 102. https://doi.org/10.1186/s13148-016-0268-4.

Nakamura, Kyosuke, Giulia Saredi, Jordan R. Becker, Benjamin M. Foster, Nhuong V. Nguyen, Tracey E. Beyer, Laura C. Cesa, et al. 2019. « H4K20me0 Recognition by BRCA1–BARD1 Directs Homologous Recombination to Sister Chromatids ». *Nature Cell Biology* 21 (3): 311-18. https://doi.org/10.1038/s41556-019-0282-9.

Oda, Hisanobu, Michael R Hübner, David B Beck, Michiel Vermeulen, Jerard Hurwitz, David L Spector, et Danny Reinberg. 2010. « Regulation of the histone H4 monomethylase PR-Set7 by CRL4(Cdt2)-mediated PCNA-dependent degradation during DNA damage ». *Molecular Cell* 40 (3): 364-76. https://doi.org/10.1016/j.molcel.2010.10.011.

Orthwein, Alexandre, Sylvie M. Noordermeer, Marcus D. Wilson, Sébastien Landry, Radoslav I. Enchev, Alana Sherker, Meagan Munro, et al. 2015. « A Mechanism for the Suppression of Homologous Recombination in G1 Cells ». *Nature* 528 (7582): 422-26. https://doi.org/10.1038/nature16142.

Pellegrino, Stefania, Jone Michelena, Federico Teloni, Ralph Imhof, et Matthias Altmeyer. 2017. « Replication-Coupled Dilution of H4K20me2 Guides 53BP1 to Pre-Replicative Chromatin ». *Cell Reports* 19 (9): 1819-31. https://doi.org/10.1016/j.celrep.2017.05.016.

Ribeyre, Cyril, Ralph Zellweger, Maeva Chauvin, Nicole Bec, Christian Larroque, Massimo Lopes, et Angelos Constantinou. 2016. « Nascent DNA Proteomics Reveals a Chromatin Remodeler Required for Topoisomerase I Loading at Replication Forks ». *Cell Reports* 15 (2): 300-309. https://doi.org/10.1016/j.celrep.2016.03.027.

Rice, Judd C, Kenichi Nishioka, Kavitha Sarma, Ruth Steward, Danny Reinberg, et C David Allis. 2002. « Mitotic-specific methylation of histone H4 Lys 20 follows increased PR-Set7 expression and its localization to mitotic chromosomes ». *Genes & development* 16 (17): 2225-30.

Saredi, Giulia, Hongda Huang, Colin M. Hammond, Constance Alabert, Simon Bekker-Jensen, Ignasi Forne, Nazaret Reverón-Gómez, et al. 2016. « H4K20me0 Marks Post-Replicative Chromatin and Recruits the TONSL–MMS22L DNA Repair Complex ». *Nature* 534 (7609): 714-18. https://doi.org/10.1038/nature18312.

Savage, Kienan I., et D. Paul Harkin. 2015. « BRCA1, a “complex” Protein Involved in the Maintenance of Genomic Stability ». *The FEBS Journal* 282 (4): 630-46. https://doi.org/10.1111/febs.13150.

Schotta, Gunnar, Roopsha Sengupta, Stefan Kubicek, Stephen Malin, Monika Kauer, Elsa Callén, Arkady Celeste, et al. 2008. « A chromatin-wide transition to H4K20 monomethylation impairs genome integrity and programmed DNA rearrangements in the mouse ». *Genes & Development* 22 (15): 2048-61. https://doi.org/10.1101/gad.476008.

Scully, Ralph, Arvind Panday, Rajula Elango, et Nicholas A. Willis. 2019. « DNA Double-Strand Break Repair-Pathway Choice in Somatic Mammalian Cells ». *Nature Reviews Molecular Cell Biology* 20 (11): 698-714. https://doi.org/10.1038/s41580-019-0152-0.

Shevchenko, Andrej, Henrik Tomas, Jan Havlis, Jesper V. Olsen, et Matthias Mann. 2006. « In-Gel Digestion for Mass Spectrometric Characterization of Proteins and Proteomes ». *Nature Protocols* 1 (6): 2856-60. https://doi.org/10.1038/nprot.2006.468.

Shilov, Ignat V., Sean L. Seymour, Alpesh A. Patel, Alex Loboda, Wilfred H. Tang, Sean P. Keating, Christie L. Hunter, Lydia M. Nuwaysir, et Daniel A. Schaeffer. 2007. « The Paragon Algorithm, a next Generation Search Engine That Uses Sequence Temperature Values and Feature Probabilities to Identify Peptides from Tandem Mass Spectra ». *Molecular & Cellular Proteomics: MCP* 6 (9): 1638-55. https://doi.org/10.1074/mcp.T600050-MCP200.

Shoaib, Muhammad, David Walter, Peter J. Gillespie, Fanny Izard, Birthe Fahrenkrog, David Lleres, Mads Lerdrup, et al. 2018. « Histone H4K20 Methylation Mediated Chromatin Compaction Threshold Ensures Genome Integrity by Limiting DNA Replication Licensing ». *Nature Communications* 9 (1): 3704.

https://doi.org/10.1038/s41467-018-06066-8.

Svobodová Kovaříková, Alena, Soňa Legartová, Jana Krejčí, et Eva Bártová. 2018. « H3K9me3 and H4K20me3 Represent the Epigenetic Landscape for 53BP1 Binding to DNA Lesions ». *Aging* 10 (10): 2585-2605. https://doi.org/10.18632/aging.101572.

Tardat, Mathieu, Julien Brustel, Olivier Kirsh, Christine Lefevbre, Mary Callanan, Claude Sardet, et Eric Julien. 2010. « The histone H4 Lys 20 methyltransferase PR-Set7 regulates replication origins in mammalian cells ». *Nature Cell Biology* 12 (11): 1086-93. https://doi.org/10.1038/ncb2113.

Tardat, Mathieu, Rabih Murr, Zdenko Herceg, Claude Sardet, et Eric Julien. 2007. « PR-Set7-dependent lysine methylation ensures genome replication and stability through S phase ». *The Journal of cell biology* 179 (7): 1413-26.

Tarsounas, Madalena, et Patrick Sung. 2020. « The Antitumorigenic Roles of BRCA1–BARD1 in DNA Repair and Replication ». *Nature Reviews Molecular Cell Biology* 21 (5): 284-99. https://doi.org/10.1038/s41580-020-0218-z.

Toh, MingRen, et Joanne Ngeow. 2021. « Homologous Recombination Deficiency: Cancer Predispositions and Treatment Implications ». *The Oncologist* 26 (9): e1526-37. https://doi.org/10.1002/onco.13829.

Veo, Bethany, Etienne Danis, Angela Pierce, Ismail Sola, Dong Wang, Nicholas K. Foreman, Jian Jin, et al. 2019. « Combined Functional Genomic and Chemical Screens Identify SETD8 as a Therapeutic Target in MYC-Driven Medulloblastoma ».

JCI Insight 4 (1). https://doi.org/10.1172/jci.insight.122933.

Veschi, Veronica, Zhihui Liu, Ty C. Voss, Laurent Ozbun, Berkley Gryder, Chunhua Yan, Ying Hu, et al. 2017. « Epigenetic SiRNA and Chemical Screens Identify SETD8 Inhibition as a Therapeutic Strategy for P53 Activation in High-Risk Neuroblastoma ». *Cancer Cell* 31 (1): 50-63. https://doi.org/10.1016/j.ccell.2016.12.002.

Wessel, Sarah R., Kareem N. Mohni, Jessica W. Luzwick, Huzefa Dungrawala, et David Cortez. 2019. « Functional Analysis of the Replication Fork Proteome Identifies BET Proteins as PCNA Regulators ». *Cell Reports* 28 (13): 3497-3509.e4. https://doi.org/10.1016/j.celrep.2019.08.051.

Witus, Samuel R., Weixing Zhao, Peter S. Brzovic, et Rachel E. Klevit. 2022. « BRCA1/BARD1 Is a Nucleosome Reader and Writer ». *Trends in Biochemical Sciences* 47 (7): 582-95. https://doi.org/10.1016/j.tibs.2022.03.001.

Xu, Yixi, et Dongyi Xu. 2020. « Repair Pathway Choice for Double-Strand Breaks ». Édité par Qian Wu. *Essays in Biochemistry* 64 (5): 765-77. https://doi.org/10.1042/EBC20200007.

Yang, Chao, Kai Wang, YingTang Zhou, et Shao-Lin Zhang. 2021. « Histone Lysine Methyltransferase SET8 Is a Novel Therapeutic Target for Cancer Treatment ». *Drug Discovery Today* 26 (10): 2423-30. https://doi.org/10.1016/j.drudis.2021.05.004.

Yilmaz, Duygu, Audrey Furst, Karen Meaburn, Aleksandra Lezaja, Yanlin Wen,

Matthias Altmeyer, Bernardo Reina-San-Martin, et Evi Soutoglou. 2021. « Activation of Homologous Recombination in G1 Preserves Centromeric Integrity ». *Nature* 600 (7890): 748-53. https://doi.org/10.1038/s41586-021-04200-z.

Zong, Dali, Salomé Adam, Yifan Wang, Hiroyuki Sasanuma, Elsa Callén, Matilde Murga, Amanda Day, et al. 2019. « BRCA1 Haploinsufficiency Is Masked by RNF168-Mediated Chromatin Ubiquitylation ». *Molecular Cell* 73 (6): 1267-1281.e7. https://doi.org/10.1016/j.molcel.2018.12.010.

Zong, Dali, Elsa Callén, Gianluca Pegoraro, Claudia Lukas, Jiri Lukas, et André Nussenzweig. 2015. « Ectopic Expression of RNF168 and 53BP1 Increases Mutagenic but Not Physiological Non-Homologous End Joining ». *Nucleic Acids Research* 43 (10): 4950-61. https://doi.org/10.1093/nar/gkv336.

FIGURE LEGENDS

Figure 1: changes in nascent chromatin composition upon the premature switch from H4K20me0 to H4K20me1. **A**. FACS profiles of control (-Tet) and Tetracyline (+Tet) treated cells synchronized at G1/S transition by double-thymidine block (green profile) and then 3 hours (orange profile), 6 hours (blue profile) and 12 hours (red profile) after released into S-phase. (**B**) Immunoblot analysis of untreated (-Tet) and Tet-treated (+Tet) cells at each time points analyzed by FACS as shown in Figure 1A. (**C**) Immunoblot analysis of iPOND samples with and without Click-it reaction in untreated and Tet-treated cells. The samples without Click-it reaction serves as negative control of pull-down samples. PCNA and Histone H4 immunoblots serve as loading controls. Similar protein levels (input) before IPOND purification have been verified by immunoblots (not shown). (**D**) Upper panels: Venn diagrams of protein sets purified by iPOND-MS with or without click-it reaction in the control (-Tet) and tetracycline (+Tet) samples. Lower panel: Venn diagram of proteins specifically associated with EdU-labelled DNA (+ click/-click) in the control (-Tet) and treated cells (+Tet) cells. **(E)** According to the p-value in log base 10, top 5 of enriched terms across proteins set specifically gained within nascent EdU-labelled DNA upon SET8^{PIPmut} expression. (**F**) Distribution of the proteins specifically enriched within EdU-labelled DNA upon tetracycline (SET8^{PIPmut} expression) according to their unused protein score (amount of unique peptide related for each identified protein) (FDR <0.01). Proteins known to be involved in DNA repair are shown. Among them, 53BP1 and SET8 are shown in bold. (**G**) According to the p-value in log base 10, top 5 of enriched terms across proteins set specifically depleted from nascent EdU-labelled DNA upon SET8^{PIPmut} expression. (**H**) Distribution of proteins specifically depleted from EdU-labelled DNA upon SET8^{PIPmut} expression (+ Tet) according to their unused protein

score as described above. (FDR <0.01). Proteins involved in DNA repair are shown in black. Among them, BRCA1 is shown in bold.

Figure 2: SET8^{PIPmut} expression impairs HR focal accumulation during S-phase. (**A**) Representative images showing staining of 53BP1 with BARD1 (top), BRCA1 (middle), or RAD51 (bottom) in EdU positive nuclei from control (-Tet) and Set8^{PIPmut} (+ Tet). replicating cells. Scale bar = 10 µm. (**B**) Scattered box-plot representing the number of BARD1 (top left), BRCA1 (top right), RAD51 (bottom left) and 53BP1 (bottom right) foci per EdU positive nucleus from control (-Tet) and Set8^{PIPmut} (+ Tet) expressing cells. Inside the box-plot graphs, the thick line represents the median, the limit of the boxes corresponds to the 0.25 and 0.75 quartiles with whiskers showing values 1.5 times the interquartile range. n ≥ 3. ***, p <0.001. Number of nuclei per condition> 100. (**C**). Upper panel: Immunoblots showing similar expression levels of SET8 protein wild-type (WT) and mutants as indicated. Left panel: Representative images showing RAD51 and 53BP1 immunostaining in EdU positive nuclei from replicating cells expressing the different FLAG-SET8 proteins as indicated. (**D**) Bar-plot representing the percentages of EdU positive nuclei that displayed RAD51 or 53BP1 foci in replicating cells expressing the different FLAG-SET8 proteins. Data = mean ± s.d., n ≥ 3. *** p<0.001 (unpaired t-test). Number of nuclei per condition >100.

Figure 3: SET8 stabilization inhibits homologous recombination. (**A**) Representative images of RAD51, BRCA1 and 53BP1 staining in EdU positive nuclei from control (-Tet) and FLAG-Set8^{PIPmut} (+Tet) expressing cells treated with 5 or 25 nM of camptothecin during 2 hours or with vehicle (DMSO) as indicated. Scale bar = 10 µm. (**B**) Scattered box-plot representing the quantification of RAD51, BRCA1 and

53BP1 foci per EdU-positive nuclei from control (- Tet) and FLAG-Set8^{PIPmut} expressing cells (+ Tet) treated with 5 nM or 25 nM of camptothecin during 2 hours, or with vehicle (DMSO). Interquartile range and statistical significance are shown as in Figure 2A. n ≥ 3; *** p<0.001 (t test). Number of nuclei per condition and experiment >100. (**C**) Left panel: Bar-plot representing the relative efficiency of DNA repair by homologous recombination of I-SceI-induced DNA breaks as evaluated by flow cytometry using the U2OS DR-GFP cell line after expression of different FLAG-SET8 proteins as indicated. Data = mean ± s.d., n = 3. *** p<0.001 (t-test). Number of events per sample > 10 000. Right panel: immunoblots showing the similar expression of different FLAG-SET8 proteins and of MYC-tagged nuclease I-SceI in U2OS DR-GFP cells. Tubulin was used as loading control.

Figure 4: SET8-mediated inhibition of BRCA1 signaling depends on 53BP1.

(**A**). Representative images showing the staining of RAD51 and 53BP1 in EdU-positive nuclei from control and 53BP1 siRNA treated cells that were subsequent induced (+ Tet) or not (-Tet) for the expression of the FLAG-Set8^{PIPmut} protein. Scale bar = 10 µm. Right panel is the scattered box-plot representing the number of RAD51 foci per EdU positive nucleus from the same cells. Inside the box-plot graphs, the thick line represents the median, the limit of the boxes corresponds to the 0.25 and 0.75 quartiles with whiskers showing values 1.5 times the interquartile range. n=3, *** p<0.001 (**B**) Representative images showing staining of BRCA1 and 53BP1 in EdU positive nuclei from control and 53BP1 siRNA treated cells that were subsequent induced (+ Tet) or not (-Tet) for the expression of the FLAG-Set8^{PIPmut} protein. Scale bar = 10 µm. Right panel is a scattered box-plot representing the number of BRCA1 foci per EdU positive nucleus from the same cells. n=3, *** p<0.001 (**C**) Representative

images showing staining of BARD1 and 53BP1 in EdU-positive nuclei from control and 53BP1 siRNA treated cells that were subsequent induced (+ Tet) or not (-Tet) for the expression of the FLAG-Set8^{PIPmut}. Scale bar = 10 µm. Right panel is a scattered box-plot representing the number of BARD1 foci per EdU+ nucleus from the same cells as above. *** $p<0.001$. n=1, number of analyzed nuclei >100 in this experiment.

Figure 5: The pharmacological inhibition of SUV4-20H activity did not prevent 53BP1 focal accumulation and the loss HR foci on replicated chromatin upon SET8 stabilization. (**A**) Representative images showing the staining of BARD1 and 53BP1 in EdU-positive nuclei from control (- Tet) and tetracycline (+ Tet) treated inducible FLAG-SET8^{PIPmut} cells, which were previously incubated with DMSO or with 10µM of the SUV4-20H inhibitor A196 for 24 hours. Scale bar = 10 µm. (**B**) Representative images showing staining of BRCA1 and 53BP1 in EdU-positive nuclei from control (Tet) and tetracycline-treated (+ Tet) Tet-inducible FLAG-SET8^{PIPmut} cells in presence or DMSO or A196 as indicated in A. Scale bar = 10 µm. (**C**) Representative images showing staining of RAD51 and 53BP1 in EdU-positive nuclei from control (- Tet) and tetracycline-treated (+ Tet) Tet-inducible FLAG-SET8^{PIPmut} cells in presence or DMSO or A196 as indicated above Scale bar = 10 µm. (**D**) Scattered box-plots representing the number of 53BP1 foci (upper panel), BARD1 foci (middle up), BRCA1 foci (middle down) and RAD51 foci (lowest panel) per EdU positive nucleus from control (- Tet) and FLAG-Set8^{PIPmut} (+ Tet) expressing cells that were incubated with DMSO or A196 as indicated above. Statistical significance was detected when a Student's test (t-test) was performed with $p<0.001$. Inside the box-plot graphs, the thick line represents the median, the limit of the boxes corresponds to the 0.25 and

0.75 quartiles with whiskers showing values 1.5 times the interquartile range interquartile range. n=3. Number of nuclei per experiment > 100. * p<0.05; *** p<0.001.

Figure 6: RNF168 and chromatin ubiquitination contribute 53BP1 focal accumulation upon SET8 stabilization. (A). Upper panels are representative images of the staining of RNF168 and 53BP1 in EdU-positive nuclei from untreated (- Tet) and tetracycline-treated (+Tet) Tet-inducible FLAG-SET8^{PIPmut} cells. Scale bar = 10 µm. Lower panels are scattered box-plots representing the number (left) and area (right) of RNF168 foci in EdU-positive nuclei from untreated (- Tet) and tetracycline-treated (+Tet) Tet-inducible FLAG-SET8^{PIPmut} cells. number of nuclei >100 per experiment; n=2. *** p<0.001**. (B).** Upper panels are representative images showing the staining of chromatin ubiquitination (FK2) and 53BP1 in EdU-positive nuclei from untreated (- Tet) and tetracycline-treated (+Tet) Tet-inducible FLAG-SET8^{PIPmut} cells. Scale bar = 10 µm. Lower panel are scattered box-plots representing the number (left) and area (right) of chromatin ubiquitination (FK2) foci in EdU-positive nuclei from untreated (- Tet) and tetracycline-treated (+Tet) Tet-inducible FLAG-SET8^{PIPmut} cells. n=1 and number of analyzed nuclei >100 in this experiment; *** p<0.001. **(C)** Representative images of the staining of 53BP1, BRCA1 and RAD51 in EdU-positive nuclei from untreated (- Tet) and tetracycline-treated (+Tet) Tet-inducible FLAG-SET8^{PIPmut} cells that were transfected with control or RNF168 siRNA two days before tetracycline treatment. Scale bar = 10 µm. n=2. **(D)** Scattered box-plot representing the number of 53PB1 foci in the nuclei as indicated in C. n=2, Number of nuclei >100 per experiment. *** p<0.001. (**E)** scattered box-plot representing the number of RAD51 and BRCA1 foci in the nuclei as indicated in C. number of nuclei >100 per experiment. ** p<0.01; *** p<0.001.

Figure 7: BRCA1 accumulation on chromatin upon SET8 depletion triggers cell-cycle defects. (**A)**. Representative immunoblots showing the localization of BRCA1 and 53BP1 in soluble cytoplasmic (S1) and nuclei (S2) fractions and in chromatin-enriched fractions (P3) at early G1 phase in control and SET8 SiRNA-treated cells that excited from mitosis without SET8 and the conversion of H4K20me0 to H4K20me1 as shown in supplementary figure S7. Cells were harvested 15 hours after G1/S release. n=3 (**B**) FACS analysis of DNA content and BrdU signal after mitotic exit of the control and SET8 SiRNA-treated cells as described above. Cells were harvested 24 hours after G1/S release. n=3 (**C**) Representative images showing EdU incorporation (DNA synthesis) and staining of 53BP1 and BRCA1 in control and siRNA SET8 treated cells progressing from G1 to S-phase after a first mitosis without SET8 and H4K20me1 as described above. Scale bar = 10 µm (**D**). FACS analysis of DNA content and BrdU incorporation levels of control (shLuc/siCtrl), SET8-depleted U2OS cells (shRNA SET8/siRNA Ctrl), BRCA1-depleted U2OS cells (shRNA Luc/siRNA BRCA1) and cells depleted for both BRCA1 and SET8 (shRNA SET8/siRNA BRCA1). n=3. Number of of events per sample > 10 000.

LEGENDS OF SUPPLEMENTARY FIGURES

Figure S1: FLAG-SET8^{PIPmut} expression during S-phase inhibits homologous recombination. (**A**). left panel: Immunoblots showing the levels of FLAG-SET8^{PIPmut} mutant after addition of tetracycline to the cell culture medium during 6 hours (+ Tet). Tubulin was used as loading control. Right panel: bar-plot representing the percentages of EdU positive nuclei that showed BARD1, BRCA1, RAD51 and/or 53BP1 foci as indicated in control (- Tet) and tetracyclin (+ Tet) inducible FLAG-

Set8^{PIPmut} cells. Data = mean ± s.d., n=3. ** p<0.01 ; *** p<0.001 (t-test). number of nuclei >100 per experiment. (**B**). Scattered box-plot representing the 53BP1 foci area in EdU positive nuclei from control (-Tet) and tetracyclin-treated (+ Tet) Tet-inducible FLAG-SET8^{PIPmut} cells. ** p<0.01; *** p<0.001. Inside the box-plot graphs, the thick line represents the median, the limit of the boxes corresponds to the 0.25 and 0.75 quartiles with whiskers showing values 1.5 times the interquartile range.n ≥ 3. *** p<0.001 (t-test), number of nuclei >100 per experiment. (**C**) Bar-plot representing the percentages of EdU positive nuclei displaying γH2AX and/or 53BP1 foci as indicated control (- Tet) and FLAG-SET8^{PIPmut} (+ Tet) cells. Data = mean ± s.d., n=3. * p<0.05; ** p<0.01; *** p<0.001. number of nuclei >100 per experiment. (**D**). Left panel: scattered box-plot representing the number of γH2AX foci per EdU positive nucleus from control (-Tet) and FLAG-Set8^{PIPmut} expressing cells (+ Tet). Right panel: Box-plot representing the γH2AX foci area in EdU positive nuclei from control (-Tet) and FLAG-SET8^{PIPmut} expressing cells (+ Tet). *** p<0.001. Inside the box-plot graphs, the thick line represents the median, the limit of the boxes corresponds to the 0.25 and 0.75 quartiles with whiskers showing values 1.5 times the interquartile range. n≥3. *** p<0.001 (t-test). number of nuclei >100 per experiment.

Figure S2: Characterization of the camptothecin-induced DNA damage responses in control and FLAG-SET8^{PIPmut} expressing cells. (**A)**. Western-blot showing the expression and phosphorylation levels of indicated proteins in control (-Tet) and FLAG-SET8^{PIPmut} (+ Tet) cells, untreated (DMSO) or treated with 5 nM or 25 nM of camptothecin during 2 hours. Tubulin was used as loading control. (**B**). Upper panel: representative images of the RPA70 and 53BP1 staining in control (- Tet) or FLAG-SET8^{PIPmut} (+ Tet) cells and that were untreated (DMSO) or treated with 25 nM

of camptothecin during 2 hours. Scale bar = 10 µm. Lower panel: Scattered box-plot representing the number of RPA foci per EdU positive nucleus from control (- Tet) and FLAG-SET8^{PIPmut} expressing cells (+ Tet) treated with 25 nM of camptothecin during 2 hours. number of nuclei >100 per experiment.

Figure S3: 53BP1 depletion in FLAG-SET8^{PIPmut} U2OS cells. Immunoblots showing the efficiency of siRNA-mediated depletion of 53BP1 and expression of the FLAG-SET8^{PIPmut} protein in untreated (- Tet) and FLAG-SET8^{PIPmut} (+Tet) cells. Tubulin was used as loading control.

Figure S4: Levels of H4K20me states in FLAG-SET8^{PIPmut} U2OS cells treated with the SUV4-20H inhibitor A196 for 24 hours. Immunoblots showing mono-, di- and trimethylation states levels of H4K20, and FLAG-SET8^{PIPmut} expression in FLAG-SET8^{PIPmut} U2OS cells co-treated or not with tetracyline and/or the SUV4-20H inhibitor A196 for 24 hours. Histone H4 and Tubulin were used as loading controls.

Figure S5: Prolonged inhibition of SUV4-20H enzymes did not prevent 53BP1 focal accumulation and did not restore HR foci in FLAG-SET8^{PIPmut} cells. (**A**). immunblots showing mono-, di- and trimethylation states levels of H4K20, and FLAG-Set8^{PIPmut} expression in control (- Tet) and FLAG-SET8^{PIPmut} (+Tet) cells that were treated (A196) or not (DMSO) with 10 µM of the SUV4-20H inhibitor A196 during 6 days. Histone 4 and Tubulin were used as loading controls. (**B**) Representative images showing staining of RAD51 and 53BP1 in EdU positive nuclei from control (- Tet) and FLAG-SET8^{PIPmut} expressing cells (+ Tet), and which were previously treated or not with 10µM of the SUV4-20H inhibitor A196 during 6 days. Scale bar = 10 µm. (**C**)

Scattered box-plots representing the number of BARD1, BRCA1, 53BP1 or RAD51 foci per EdU positive nucleus from control (- Tet) and FLAG-SET8^{PIPmut} replicating cells (+ Tet) that were previously treated (A196) or not (DMSO) with 10μM of A196 during 6 days. Inside the box-plot graphs, the thick line represents the median, the limit of the boxes corresponds to the 0.25 and 0.75 quartiles with whiskers showing values 1.5 times the interquartile range. n=3. * $p<0.05$; **$p<0.001$ (t-test). number of nuclei >100 per experiment.

Figure S6: RNF168 recruitment on replicated chromatin upon SET8 stabilization. (**A**) Bar-plot representing the percentages of EdU positive nuclei displaying RNF168 and/or 53BP1 nuclear foci in control (-Tet) and FLAG-SET8^{PIPmut} (+Tet) cells. Data = mean ± s.d., n =3. *$p<0.05$; ***$p<0.001$ (t-test). number of nuclei >100 per experiment **(B)** Upper panels are representative images of RNF168 and 53BP1 staining in EdU-positive nuclei from untreated (-Tet) and FLAG-Set8^{PIPmut} (+Tet) cells, two hours after exposure of not with camptothecin as indicated. lower panel: Scattered box-plots representing the number of RNF168 foci per EdU-positive nucleus from untreated (-Tet) and FLAG-Set8^{PIPmut} (+Tet) cells after exposure of not with camptothecin as indicated. Inside the box-plot graphs, the thick line represents the median, the limit of the boxes corresponds to the 0.25 and 0.75 quartiles with whiskers showing values 1.5 times the interquartile range. ***$p<0.001$**.** Number of nuclei per condition and per experiment > 100**. (C)** Scattered box-plot representing the number of RNF168 foci per EdU positive nucleus from control and 53BP1 depleted Tet-inducible FLAG-SET8^{PIPmut} cells that were subsequent induced (+ Tet) or not (-Tet) for the expression of the FLAG-SET8^{PIPmut} protein for 24 hours. the thick line represents the median, the limit of the boxes corresponds to the 0.25 and 0.75 quartiles with whiskers showing values

1.5 times the interquartile range. ***p<0.001 **(D)** Scattered box-plots representing the number or RNF168 foci per EdU positive nucleus of Tet-inducible FLAG-SET8^{PIPmut} cells untreated (-Tet) or treated with tetracycline (+Tet) in presence or not of the Suv4-20h pharmacological inhibitor A196 (10 µM, 24h). The thick line represents the median, the limit of the boxes corresponds to the 0.25 and 0.75 quartiles with whiskers showing values 1.5 times the interquartile range. * p<0.05; ***p<0.001. Number of nuclei per condition and per experiment > 100. **(E)** Immunoblots showing the levels of RNF168 and FLAG-SET8^{PIPmut} protein in control (-Tet) and SET8^{PIPmut} (+ Tet) cells that were previously transfected with control or RNF168 siRNA two days before tetracycline treatment. Tubulin was used as loading control.

Figure S7: G1/S synchronization followed by SET8 depletion prevents the switch from H4K20me0 to H4K20me1 after DNA replication. Upper panel is a cartoon showing the synchronization protocol. U2OS were synchronized with double thymidine block at G1/S transition, control and SET8 siRNA transfected 12h before G1/S release. Cells were then collected at different time points and cell-cycle progression was analyzed by FACS (lower panels). Proteins levels at each time points were analyzed by immunoblots (right panels).

ACKNOWLEDGMENTS

This work was supported by Agence Nationale pour la Recherche (ANR-20-CE12-000 -LysMeth to E.J.), SIRIC Montpellier Cancer grant (to E.J.) and ligue contre le cancer Languedoc Roussillon (520027FF to CG). Institutional Support was provided by the Institut National de la Santé et de la Recherche Médicale (INSERM), by the Centre National de la Recherche Scientifique (CNRS). Y.P. was supported by a fellowship from Ligue Nationale Contre le Cancer (LNCC), F.A. by a fellowship from Université Montpelllier (UM)/CNRS-Liban and by LNCC. We thank Christian Larroque and Alain Mange for advices in MS analysis and Florence Cammas for helpful conceptual advices.

AUTHORS CONTRIBUTION

YP, CG and EJ designed the project, CG and EJ supervised the research. YP, CG, JP, VB, FA, DL and EJ performed the experiments. YP, CG, FA, VB, CR, and EJ analyzed the data. CR, VB and DL provided conceptual advices. EJ wrote the paper with the help of ML, VB, YP and CG for figure legends and material and methods. YP, CG, DL, VB and CR contributed to manuscript editing. YP and MR performed MS experiments. YP, ML and EJ performed MS analysis.

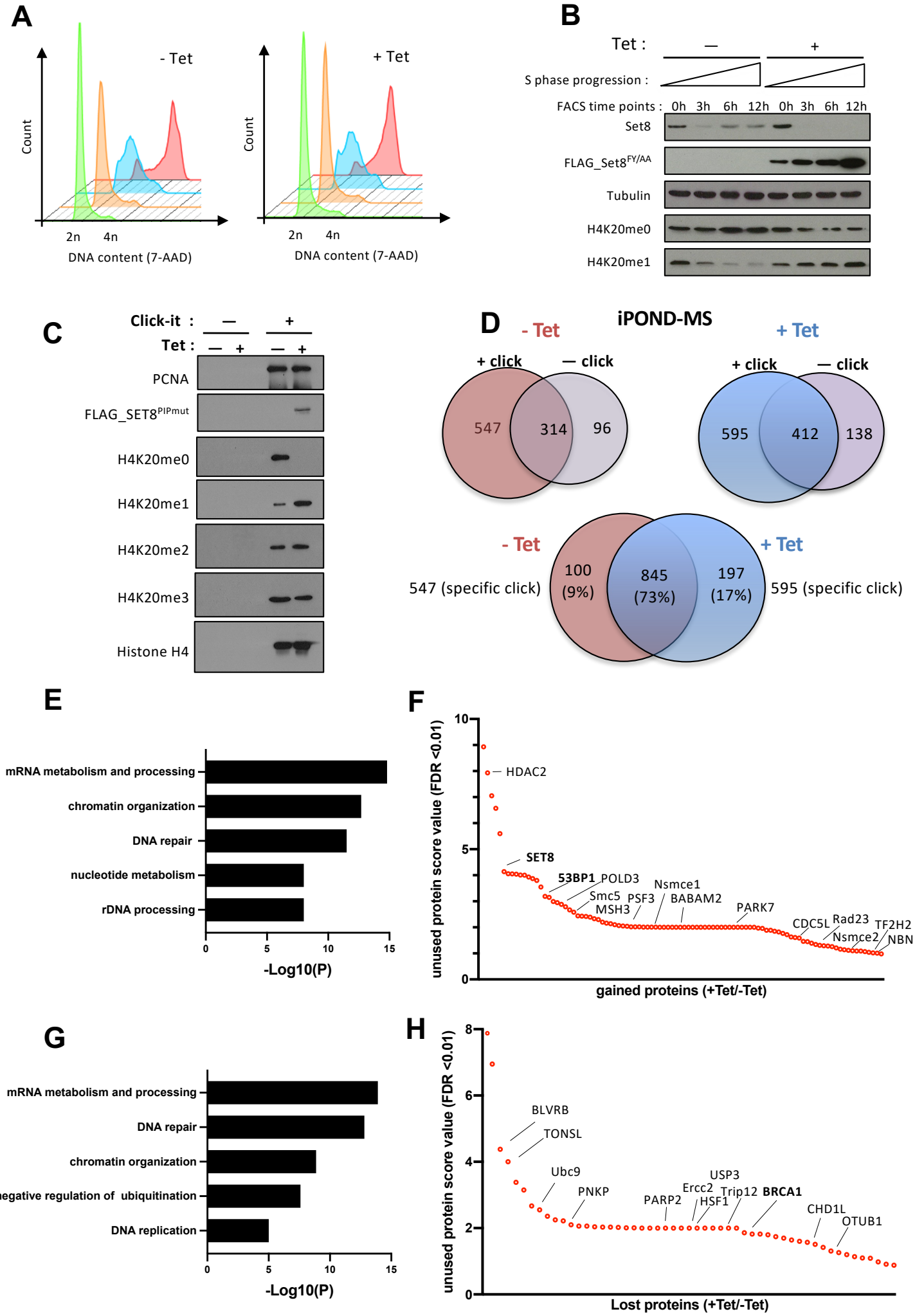
A
- Tet
+ Tet
Count
2n
4n
DNA content (7-AAD)
B
Tet :
—
+
S phase progression :
FACS time points : 0h 3h 6h 12h 0h 3h 6h 12h
Set8
FLAG_Set8FY/AA
Tubulin
H4K20me0
H4K20me1
C
Click-it : — +
Tet : — + — +
PCNA
FLAG_SET8PIPmut
H4K20me0
H4K20me1
H4K20me2
H4K20me3
Histone H4
D
iPOND-MS
- Tet
+ Tet
+ click
— click
547
314
96
595
412
138
547 (specific click)
100 (9%)
845 (73%)
197 (17%)
595 (specific click)
E
mRNA metabolism and processing
chromatin organization
DNA repair
nucleotide metabolism
rDNA processing
-Log10(P)
F
unused protein score value (FDR <0.01)
HDAC2
SET8
53BP1
POLD3
Smc5
MSH3
PSF3
Nsmce1
BABAM2
PARK7
CDC5L
Rad23
Nsmce2
TF2H2
NBN
gained proteins (+Tet/-Tet)
G
mRNA metabolism and processing
DNA repair
chromatin organization
negative regulation of ubiquitination
DNA replication
-Log10(P)
H
unused protein score value (FDR <0.01)
BLVRB
TONSL
Ubc9
PNKP
PARP2
Ercc2
USP3
HSF1
Trip12
BRCA1
CHD1L
OTUB1
Lost proteins (+Tet/-Tet)

FIGURE 1

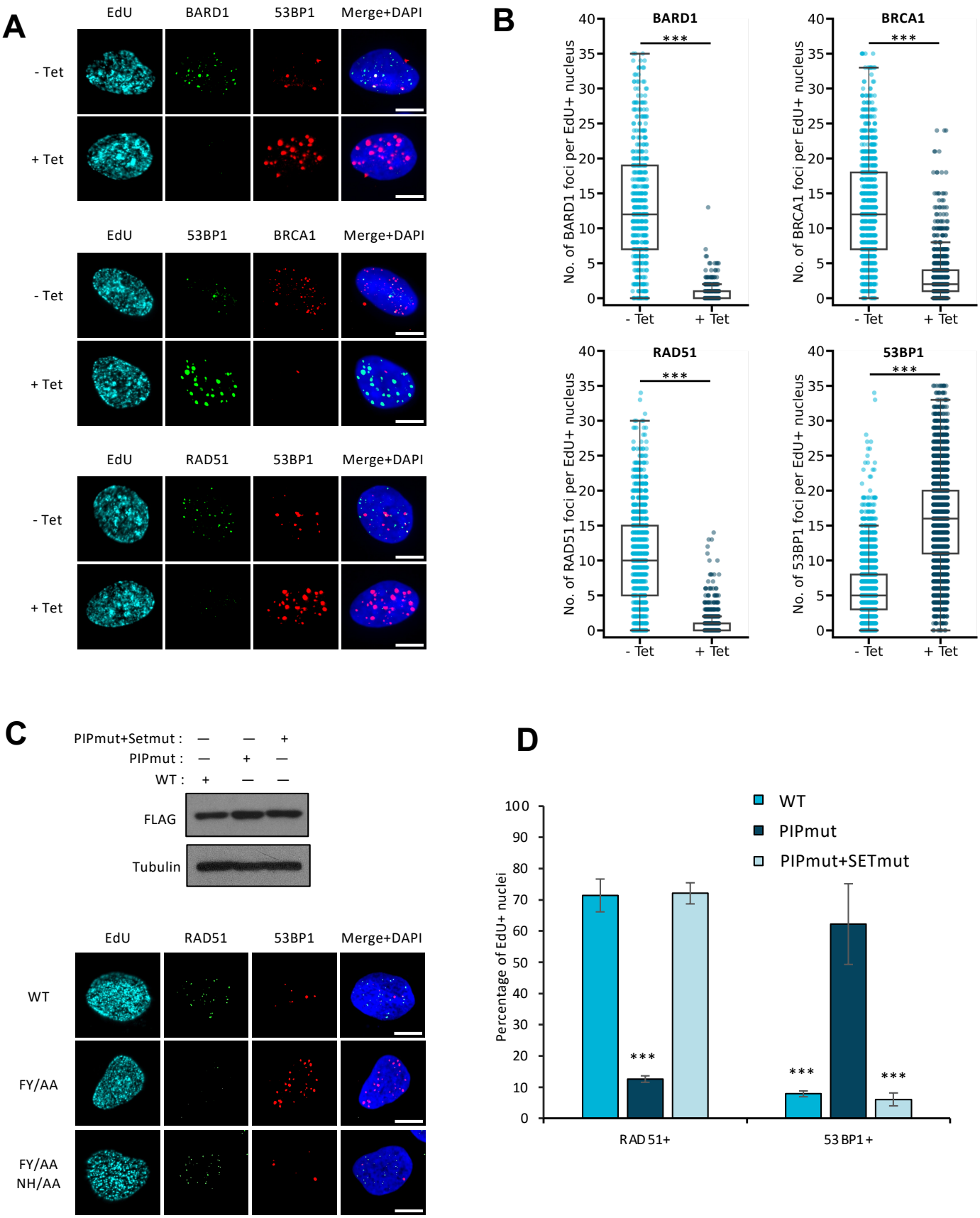
A
EdU
BARD1
53BP1
Merge+DAPI
- Tet
+ Tet
EdU
53BP1
BRCA1
Merge+DAPI
- Tet
+ Tet
EdU
RAD51
53BP1
Merge+DAPI
- Tet
+ Tet
B
BARD1
BRCA1
RAD51
53BP1
***
No. of BARD1 foci per EdU+ nucleus
No. of BRCA1 foci per EdU+ nucleus
No. of RAD51 foci per EdU+ nucleus
No. of 53BP1 foci per EdU+ nucleus
0
5
10
15
20
25
30
35
40
- Tet
+ Tet
C
PIPmut+Setmut :
PIPmut :
WT :
FLAG
Tubulin
EdU
RAD51
53BP1
Merge+DAPI
WT
FY/AA
FY/AA
NH/AA
D
WT
PIPmut
PIPmut+SETmut
Percentage of EdU+ nuclei
0
10
20
30
40
50
60
70
80
90
100
***
RAD51+
53BP1+

FIGURE 2

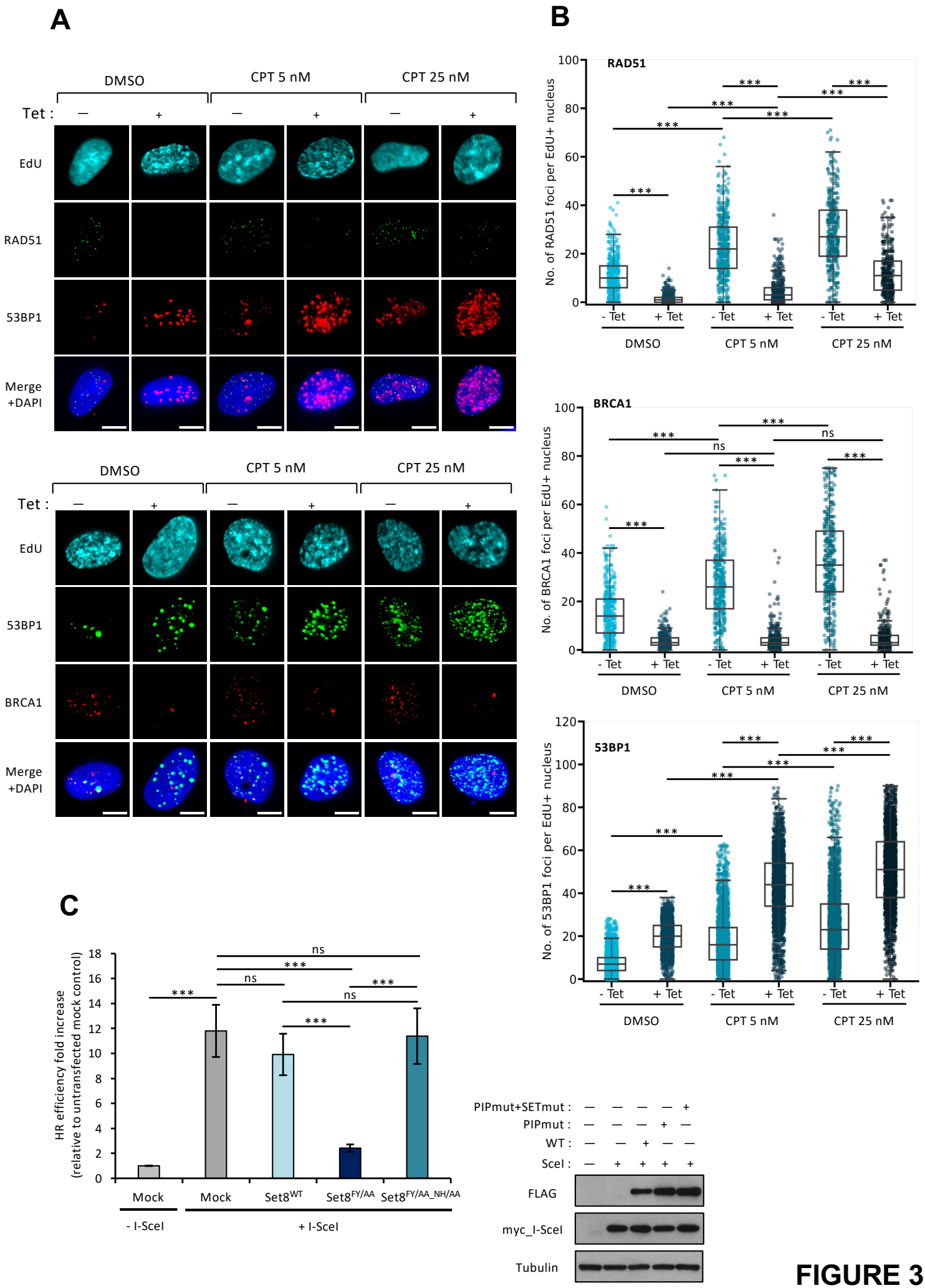
A
DMSO
CPT 5 nM
CPT 25 nM
Tet :
EdU
RAD51
53BP1
Merge +DAPI
BRCA1
B
RAD51
No. of RAD51 foci per EdU+ nucleus
BRCA1
No. of BRCA1 foci per EdU+ nucleus
53BP1
No. of 53BP1 foci per EdU+ nucleus
- Tet
+ Tet
ns
C
HR efficiency fold increase (relative to untransfected mock control)
Mock
Set8WT
Set8FY/AA
Set8FY/AA_NH/AA
- I-SceI
+ I-SceI
PIPmut+SETmut :
PIPmut :
WT :
SceI :
FLAG
myc_I-SceI
Tubulin

FIGURE 3

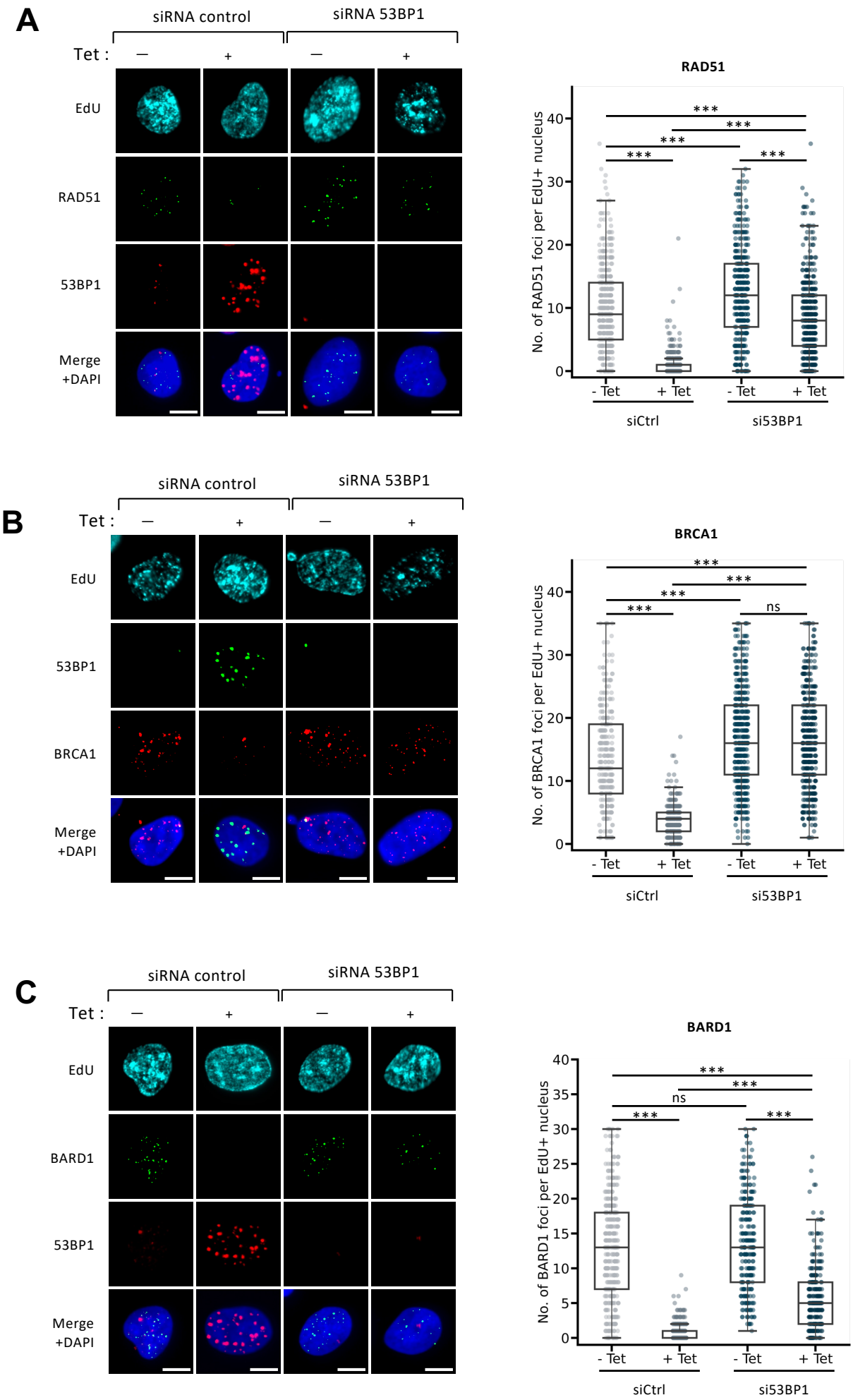
A
siRNA control
siRNA 53BP1
Tet :
–
+
–
+
EdU
RAD51
53BP1
Merge
+DAPI
RAD51
No. of RAD51 foci per EdU+ nucleus
***
***
***
***
- Tet
+ Tet
- Tet
+ Tet
siCtrl
si53BP1
B
siRNA control
siRNA 53BP1
Tet :
–
+
–
+
EdU
53BP1
BRCA1
Merge
+DAPI
BRCA1
No. of BRCA1 foci per EdU+ nucleus
***
***
***
***
ns
- Tet
+ Tet
- Tet
+ Tet
siCtrl
si53BP1
C
siRNA control
siRNA 53BP1
Tet :
–
+
–
+
EdU
BARD1
53BP1
Merge
+DAPI
BARD1
No. of BARD1 foci per EdU+ nucleus
***
***
ns
***
***
- Tet
+ Tet
- Tet
+ Tet
siCtrl
si53BP1

FIGURE 4

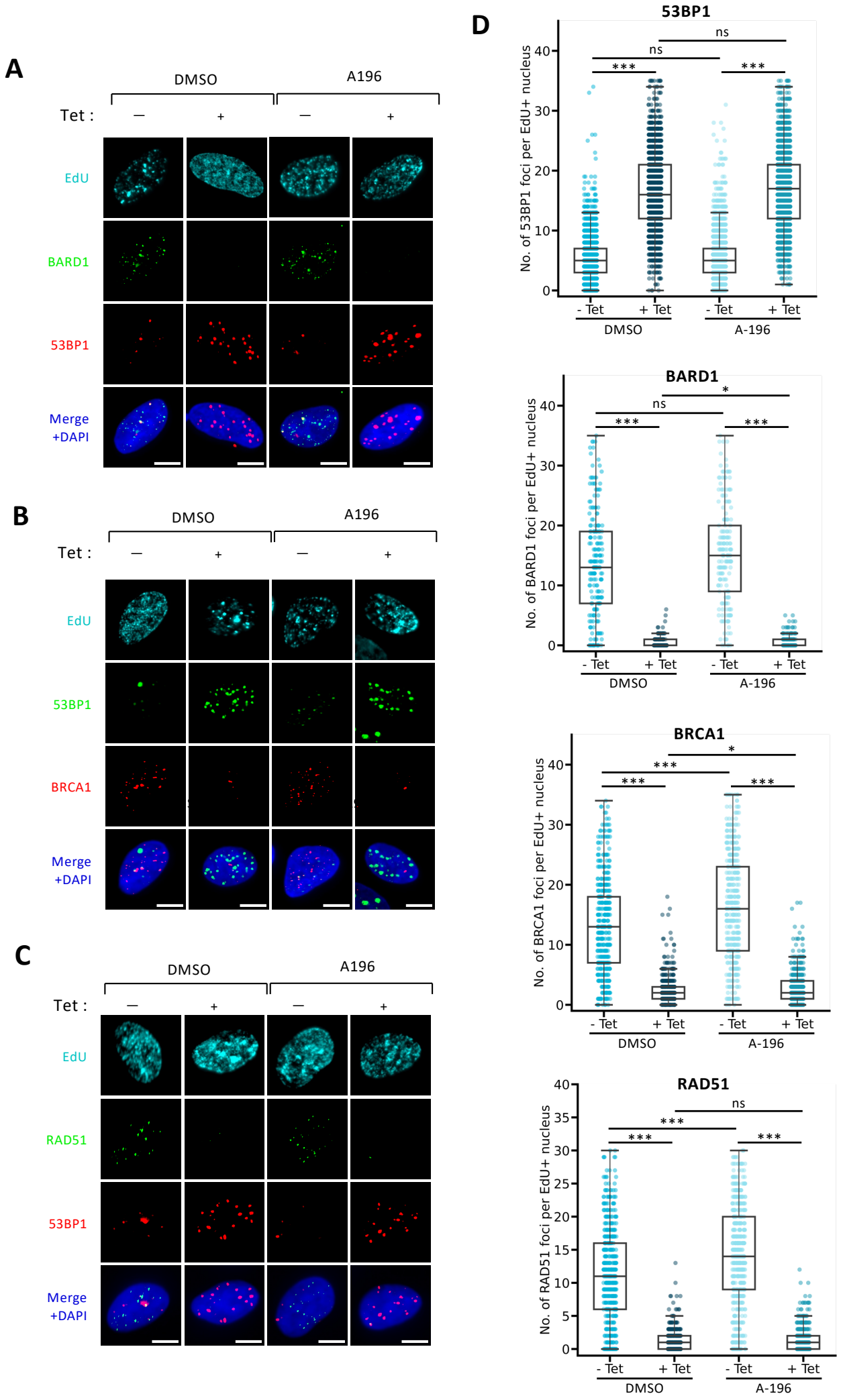
A
DMSO
A196
Tet :
–
+
–
+
EdU
BARD1
53BP1
Merge
+DAPI
B
DMSO
A196
Tet :
–
+
–
+
EdU
53BP1
BRCA1
Merge
+DAPI
C
DMSO
A196
Tet :
–
+
–
+
EdU
RAD51
53BP1
Merge
+DAPI
D
53BP1
No. of 53BP1 foci per EdU+ nucleus
ns
ns
***
***
- Tet
+ Tet
- Tet
+ Tet
DMSO
A-196
BARD1
No. of BARD1 foci per EdU+ nucleus
*
ns
***
***
- Tet
+ Tet
- Tet
+ Tet
DMSO
A-196
BRCA1
No. of BRCA1 foci per EdU+ nucleus
*
***
***
***
- Tet
+ Tet
- Tet
+ Tet
DMSO
A-196
RAD51
No. of RAD51 foci per EdU+ nucleus
ns
***
***
***
- Tet
+ Tet
- Tet
+ Tet
DMSO
A-196

FIGURE 5

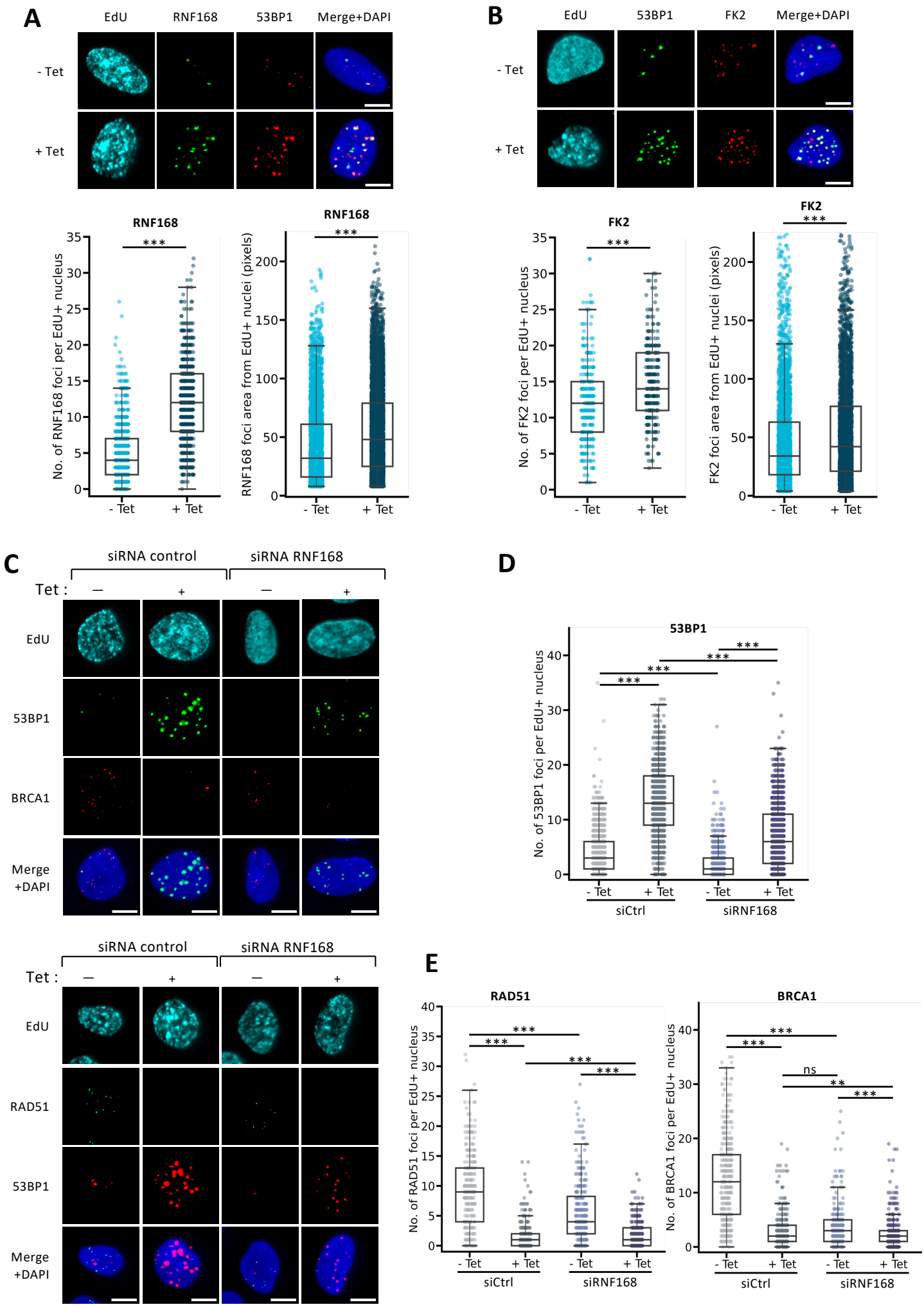
A
EdU
RNF168
53BP1
Merge+DAPI
- Tet
+ Tet
RNF168
No. of RNF168 foci per EdU+ nucleus
RNF168 foci area from EdU+ nuclei (pixels)
***
- Tet
+ Tet
B
EdU
53BP1
FK2
Merge+DAPI
FK2
No. of FK2 foci per EdU+ nucleus
FK2 foci area from EdU+ nuclei (pixels)
C
siRNA control
siRNA RNF168
Tet :
EdU
53BP1
BRCA1
Merge +DAPI
RAD51
D
53BP1
No. of 53BP1 foci per EdU+ nucleus
siCtrl
siRNF168
E
RAD51
No. of RAD51 foci per EdU+ nucleus
BRCA1
No. of BRCA1 foci per EdU+ nucleus
ns
**

FIGURE 6

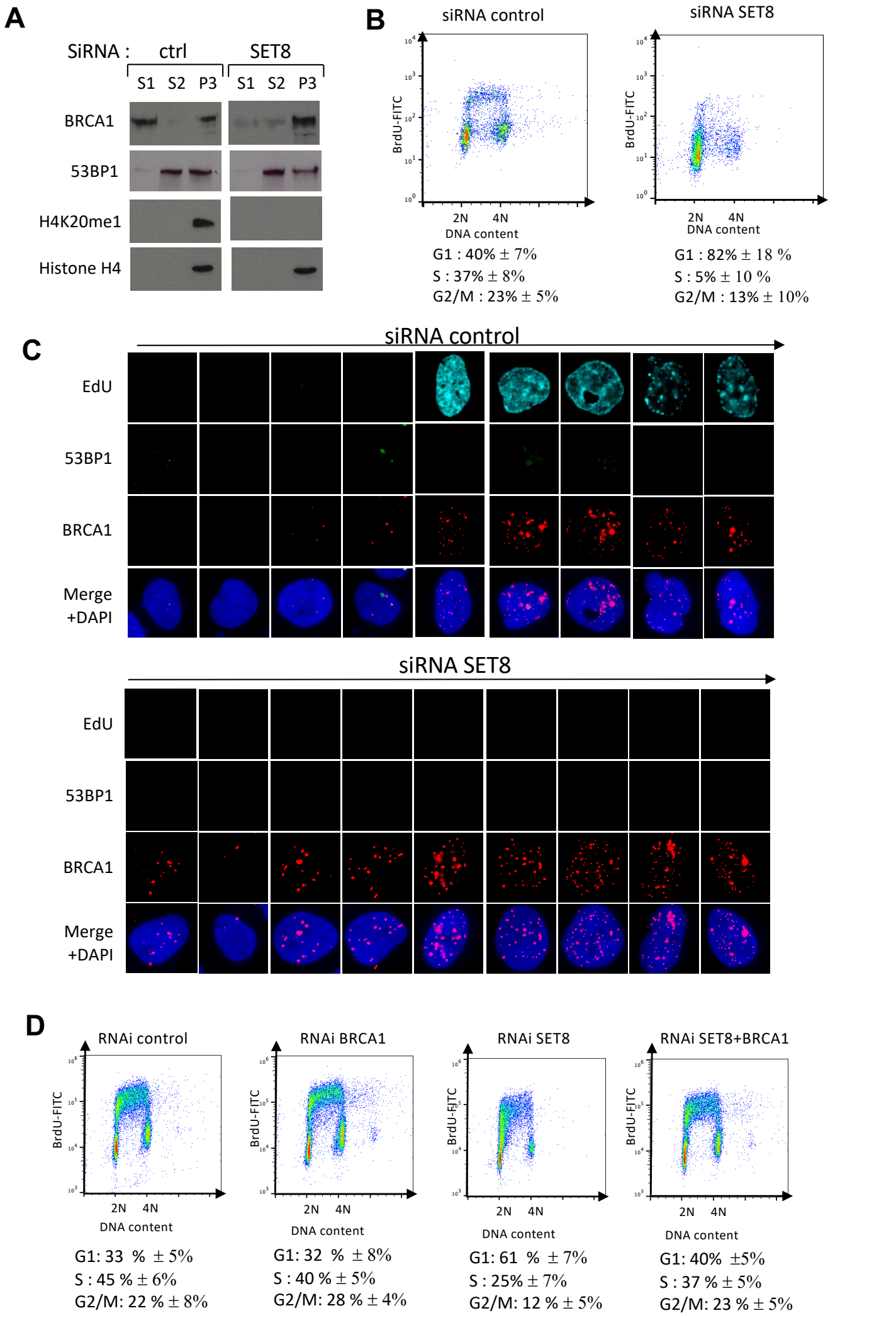
A
SiRNA : ctrl SET8
S1 S2 P3 S1 S2 P3
BRCA1
53BP1
H4K20me1
Histone H4
B
siRNA control
siRNA SET8
BrdU-FITC
2N 4N
DNA content
G1 : 40% ± 7%
S : 37% ± 8%
G2/M : 23% ± 5%
G1 : 82% ± 18 %
S : 5% ± 10 %
G2/M : 13% ± 10%
C
siRNA control
EdU
53BP1
BRCA1
Merge +DAPI
siRNA SET8
EdU
53BP1
BRCA1
Merge +DAPI
D
RNAi control
RNAi BRCA1
RNAi SET8
RNAi SET8+BRCA1
BrdU-FITC
2N 4N
DNA content
G1: 33 % ± 5%
S : 45 % ± 6%
G2/M: 22 % ± 8%
G1: 32 % ± 8%
S : 40 % ± 5%
G2/M: 28 % ± 4%
G1: 61 % ± 7%
S : 25% ± 7%
G2/M: 12 % ± 5%
G1: 40% ±5%
S : 37 % ± 5%
G2/M: 23 % ± 5%

FIGURE 7